2

Technical Report No. AE 73-1

CR 114656
AVAILABLE TO THE PUBLIC

Department of Aerospace Engineering
University of Maryland, College Park

(NASA-CR-114656) TWO-DIMENSIONAL LAMINAR INCOMPRESSIBLE SEPARATED FLOW PAST AIRFOILS (Maryland Univ.) 82 p HC $6.25 CSCL 20D

N73-29185

Unclas
G3/12 11617

Two-Dimensional Laminar Incompressible Separated Flow Past Airfoils

A. Plotkin

This research was supported by NASA under Research Grant No. NGR 21-002-266 Supplement No. 1

SEP 1973
RECEIVED
NASA-STI FACILITY
INPUT BRANCH

Distribution of this report is unlimited

July 1973

DEPARTMENT OF AEROSPACE ENGINEERING

UNIVERSITY OF MARYLAND, COLLEGE PARK

Technical Report No. AE 73-1

TWO-DIMENSIONAL LAMINAR INCOMPRESSIBLE SEPARATED FLOW PAST AIRFOILS

By

Allen Plotkin
Associate Professor

July 1973

This research was supported by NASA under Research Grant No. NGR 21-002-266 Supplement No. 1

PRECEDING PAGE BLANK NOT FILMED

ACKNOWLEDGMENTS

This research was supported by the Large Scale Aerodynamics Branch of NASA-Ames Research Center under Grant NGR 21-002-266, Supplement No. 1. A portion of the computer time was provided by the Computer Science Center of the University of Maryland.

The computer programming was performed by K.N. Parthasarathy and R. Khatri who were supported in part by the Minta Martin Fund of the University of Maryland.

The author wishes to thank J. Klineberg of NASA-Ames Research Center for many valuable technical discussions.

ABSTRACT

In this report a method is proposed to treat the problem of steady, two-dimensional, laminar, incompressible, high Reynolds number separated flow past thin airfoils. An integral form of the boundary-layer equations with interaction is used and the interaction between the inviscid and viscous flowfields is provided for by use of a thin-airfoil integral. A detailed documentation of the attempts at obtaining a solution is presented. Even though these attempts were essentially unsuccessful, they help to suggest paths for future research on this difficult problem. In addition, a useful survey of the current state-of-the-art of problems involving viscous-inviscid interactions in flow-fields with separation is given.

TABLE OF CONTENTS

Chapter		Page
I	Introduction	1
II	Mathematical Formulation of Problem	6
	A. Viscous Region	6
	B. The Interaction Equation	10
	C. Matching Conditions	12
	D. Airfoil and Initial Potential Flow Solution	13
III	Methods of Solution	15
	A. Karman-Pohlhausen in Airfoil Forward Portion	15
	B. Weak Interaction Equations in Airfoil Forward Portion	18
	C. Velocity Dependent Interaction Equation	21
	D. Updating of Solution in Airfoil Forward Portion	24
IV	Solution of Klineberg and Steger	27
	A. Viscous Flow	27
	B. Inviscid Flow	27
	C. Complete Interaction	28
V	Current Research in Viscous-Inviscid Interactions	31
VI	Discussion and Conclusions	38
	References	41
	Appendix A: Polynomial Curve Fits of Profile Quantities	46
	Appendix B: Von Karman Potential Flow Method	48

LIST OF TABLES

Table		Page
1	A Typical Computation for the Method of IIIA	44
2	Computation for the Method of IIIA with Starting Point at .50S	44
3	A Typical Computation for the Method of IIID	45
4	A Comparison of tan Θ at the Joining Point Calculated from the Continuity and Linking Equations	45

LIST OF FIGURES

Figure		Page
1	Coordinate System for Viscous Region	51
2	Flow Regions Distinguished by Velcoity Profile Shape	51
3	Coordinate System for Inviscid Region	52
4	Joukowski Airfoil, Its Slope and Surface Speed	53
5	Typical Inviscid Surface Speed Distribution for Method of IIIA (On Airfoil)	54
6	Typical Inviscid Surface Speed Distribution for Method of IIIA (In Wake)	55
7	Typical tan Θ Distribution for Method of IIIA	56
8	Typical Displacement Thickness Distribution for Method of IIIA (On Airfoil)	57
9	Typical Displacement Thickness Distribution for Method of IIIA (In Wake)	58
10	Solution of Weak Interaction Equations for Profile Parameter and Displacement Thickness	59
11	Inviscid Surface Speed Distributions Resulting from Initial tan Θ Distributions of Equation (21)	60
12	Updated tan Θ Distributions Resulting from Initial tan Θ Distributions of Equation (21)	61
13	Component Parts of tan Θ Integral Shown in Figure 12	62
14	Potential Flow Surface Speed Distribution Upstream of Leading Edge	63
15	Updated tan Θ Distribution Resulting from Initial tan Θ Distribution of Equation (21b) Including Upstream Correction	64
16	Von Karman Method Solution for 10% Joukowski Airfoil	65
17	Typical Airfoil Plus Displacement Thickness for Method of IIID	66
18	Typical Displacement Thickness Distribution for Method of IIID	67

Figure		Page
19	Typical Inviscid Surface Speed Distribution for Method of IIID (On Airfoil)	68
20	Typical Inviscid Surface Speed Distribution for Method of IIID (In Wake)	69
21	Computational Regions with Boundary Conditions for Method of Klineberg and Steger	70
22	Typical Distributions for Method of Klineberg and Steger	71
23	Comparison of Pressure Coefficient with Experimental Values of Collins for Method of Klineberg and Steger	71
24	Effect of Reynolds Number on Pressure Coefficient for Method of Klineberg and Steger	72
25	Effect of Mach Number on Pressure Coefficient for Method of Klineberg and Steger	72

SYMBOLS

a	Velocity profile parameter, defined on p
A_{iK}	Coefficients defined in Equation (B3)
c	Chord length
C_p	Pressure coefficient
C_k	Coefficients used in Table A1
D_1, D_2, D_3, D	Expressions defined in Equation (14)
f	Airfoil shape function
F	Dummy function in Table A1
H, J, P, R, Z	Profile shape quantities defined in Equation (8)
i, j, k	Integers
M	Mach number
n	Distance measured normal to wall
N_1, N_2, N	Expressions defined in Equation (18)
N	Number of source elements in von Karman method
p	Pressure
q, q_i	Source strength per unit length
Q_i	Normalized source strength $Q_i = q_i/2U_\infty\pi$
RSP	Wake rear stagnation point
R_{ec}	Chord Reynolds number
s	Distance along wall
S	Airfoil arclength
SEP	Separation point
u, v	Velocity components in s, n directions (viscous)
U, V	Velocity components in x,y directions (inviscid)
x, y	Coordinates for inviscid flow (see Figure 3)

Δx	Length of source interval in von Karman method
δ	Boundary-layer thickness
δ^*	Displacement thickness
$\S$	Dummy variable
ε	Airfoil thickness parameter
θ	Momentum thickness
θ^*	Energy thickness
Θ	Streamline direction at boundary-layer edge
μ	Viscosity coefficient
ν	Kinematic viscosity coefficient
ρ	Density
ϕ	Velocity potential
ψ	Stream function

Subscripts

e	Viscous layer edge
∞	Free stream

Superscripts

'	Scaling in Equation (13)
-	Perturbation quantity
$\sim$	Variable Defined in Appendix A

CHAPTER I

INTRODUCTION

The problem under consideration is the theoretical study of laminar, steady, incompressible, high Reynolds number separated flow past two-dimensional airfoils. The quantitative description of flowfields containing separation is one of the major unsolved problems of fluid mechanics. To appreciate the difficulty involved in the proposed research, consider first the laminar, incompressible, high Reynolds number flow along a rigid surface in the absence of regions of separated flow.

Prandtl demonstrated that the effects of viscosity can be considered to be confined to a narrow region - with thickness proportional to the inverse square root of the Reynolds number - close to the surface. He proposed the boundary-layer equations as an accurate approximation to the Navier-Stokes equations for flows with large values of the Reynolds number. To first order in the inverse square root of the Reynolds number, the pressure distribution does not vary across the boundary layer and may be obtained by a computation of the potential flow past the surface. The boundary-layer equations may then be integrated with this pressure distribution as a known quantity - various accurate numerical techniques are available, for example. Van Dyke[1] has shown how corrections may be added to the first-order solution to account for streamline displacement and surface curvature effects.

In the event that regions of separated flow are present along the surface of the body, the viscous layer thickens rapidly and first-order perturbations may be introduced into the outer potential flow field. This violates the result of classical boundary-layer theory that the outer flow to first order is independent of the boundary layer. With this breakdown of boundary-layer theory in the region near the separation point, it would seem that the appropriate path to follow to compute the flowfield with separation present is to integrate the complete Navier-Stokes equations.

At the time this research was initiated, it was felt that a numerical solution of the Navier-Stokes equations for this problem was beyond the state-of-the-art and up to the time of the writing of this report, this is still the case. Navier-Stokes solutions to the high Reynolds number separated flow situation are still not available although much progress is being made in the development of suitable numerical techniques. Recently, Davis[2] and Davis and Werle[3] have developed a numerical scheme for integrating the Navier-Stokes equations for flow past the parabola and paraboloid of revolution at all values of the Reynolds number. It remains to be shown whether this technique will prove suitable for the separated flow problem. Jacob[4] uses a boundary layer - inviscid outer flow iteration scheme to treat airfoil separated flow problems but uses a crude dead-water model for the separated flow and wake regions. The results compare well with available experiments. Similar treatment for the circular cylinder problem is presented in Bluston and Paulson[5].

An appropriate technique for the solution of this problem will have to allow for interaction between the outer inviscid flow and the inner viscous layer. Strong interaction problems of this type where the viscous and inviscid layers develop simultaneously have been successfully treated for the case of a supersonic outer stream by Lester Lees and co-workers at the California Institute of Technology using a method known as viscous-inviscid interaction theory. Some illustrative examples of this method are presented in Klineberg and Lees[6] and Alber[7]. In the latter, Alber outlines an approach for the solution of the incompressible turbulent wake problem.

The essential features of the viscous-inviscid interaction theory are as follows. It is assumed that the boundary-layer equations adequately describe the important features of the flow in the viscous region. Their use is modified, however, since the outer flow pressure gradient is not known in advance but is calculated simultaneously with the variables in the viscous region. The partial differential equations valid in the viscous layer are integrated across the layer and are thereby reduced to a set of ordinary differential equations. An equation is introduced to link the outer inviscid and inner viscous flowfields, and the complete set of equations is integrated with the inviscid surface speed as one of the unknowns. For the case of the supersonic outer stream, the linking equation usually is of the form of a Prandtl-Meyer relation.

At the initiation of this research, it was proposed to extend the method of viscous-inviscid interactions to allow for the solution

of the incompressible flow problem under consideration. The main task was then to develop an appropriate equation or technique to link the inviscid and viscous flow regions. This task is complicated since the inviscid flowfield is governed by an elliptic partial differential equation (Laplace's equation) for the incompressible case so that the surface speed at any body location is dependent on the complete displacement thickness distribution. It was clear that to discover the appropriateness of this technique for the solution of this problem it would be useful to choose a flow configuration which would allow for simplifying approximations in the treatment of the inviscid flowfield. A thin symmetric Joukowski airfoil seemed an ideal choice since simplifications could be introduced to take advantage of both the symmetry and the small flow disturbances. A thin-airfoil integral could then be used as the linking equation and the need to compute the detailed inviscid flowfield is removed.

In the following chapters, the method is developed and several attempts at solution are discussed. Since a solution was not obtained, it was felt most appropriate to present the results of the research in an essentially chronological sequence to allow the reader to determine the approaches attempted and their subsequent outcomes.

The problem for separated flow past biconvex airfoils has recently been solved for both subsonic and transonic flowfields by Klineberg and Steger[8] of NASA-Ames Research Center. They found it

necessary to compute the complete inviscid flowfield using the finite-difference relaxation technique developed by Steger and Klineberg[9] and to make use of an interactive computer graphics system. Also, attempts are currently underway to solve the interaction problem without resorting to an integral representation for the viscous region. Klemp and Acrivos[10] and others have developed numerical techniques for the integration of the boundary-layer equations through a reverse flow region and Erdos, Baronti and Elzweig[11] discuss the inclusion of such a technique in a method for the solution of a transonic interaction problem.

At present, research is underway to study interaction problems for flows ranging from incompressible to hypersonic and for both the laminar and turbulent cases. In this report, in addition to a description of the present research (Chapters II and III), a detailed discussion is given of the results of Klineberg and Steger[8] (Chapter IV) and a survey is presented of the current state-of-the-art in the area of viscous-inviscid interactions (Chapter V).

CHAPTER II

MATHEMATICAL FORMULATION OF PROBLEM

A. Viscous Region

Consider the two-dimensional steady laminar flow of an incompressible fluid at high Reynolds number. Classical boundary-layer theory would require a consideration of the continuity and streamwise momentum equations. For the formulation of this interaction problem, it is necessary to include the mechanical energy equation which is obtained by multiplying the streamwise momentum equation by the streamwise velocity component. The coordinate system used is shown on Figure 1. s and n are distances measured along and normal to the surface, respectively. u and v are the velocity components in the s and n directions. p is the pressure, ρ is the density and μ is the dynamic viscosity coefficient.

The governing partial differential equations are

Continuity:
$$\frac{\partial u}{\partial s} + \frac{\partial v}{\partial n} = 0 \tag{1}$$

Streamwise Momentum:
$$\rho\left(u \frac{\partial u}{\partial s} + v \frac{\partial u}{\partial n}\right) = - \frac{dp}{ds} + \mu \frac{\partial^2 u}{\partial n^2} \tag{2}$$

Mechanical Energy:
$$\rho\left(u^2 \frac{\partial u}{\partial s} + uv \frac{\partial u}{\partial n}\right) = -u \frac{dp}{ds} + \mu u \frac{\partial^2 u}{\partial n^2} \tag{3}$$

The equations are now integrated across the boundary layer, from the surface n = 0 to the boundary-layer edge n = δ. At the surface, u = v = 0. At the edge, $u = u_e(s)$, $v = v_e(s)$ and the shear stress $\mu \partial u / \partial n = 0$. The integrated equations are

$$\tan\theta \equiv \frac{v_e}{u_e} = \frac{d\delta^*}{ds} - (\delta - \delta^*)\frac{d\ell n u_e}{ds} \tag{4}$$

$$\frac{d}{ds}\, u_e^2\theta + \delta^* u_e \frac{du_e}{ds} = \mu \left.\frac{\partial u}{\partial n}\right|_{n=0}/\rho \tag{5}$$

$$\frac{d}{ds}\, u_e^3\theta^* = 2\nu \int_o^\delta \left(\frac{\partial u}{\partial n}\right)^2 dn \tag{6}$$

where $\nu = \mu/\rho$, the kinematic viscosity, θ is the streamline direction at the boundary-layer edge, and δ^*, θ and θ^* are the displacement, momentum and energy thicknesses given by

$$\begin{aligned}
\delta^* &= \int_o^\delta \left(1 - \frac{u}{u_e}\right) dn \\
\theta &= \int_o^\delta \frac{u}{u_e}\left(1 - \frac{u}{u_e}\right) dn \\
\theta^* &= \int_o^\delta \frac{u}{u_e}\left(1 - \frac{u^2}{u_e^2}\right) dn
\end{aligned} \tag{7}$$

It is convenient to introduce the following quantities which depend on the streamwise velocity profile.

$$\begin{aligned}
H &= \theta/\delta^* \\
J &= \theta^*/\delta^* \\
Z &= \frac{1}{\delta^*}\int_o^\delta \frac{u}{u_e}\, dn \\
R &= 2\delta^* \int_o^\delta \left[\frac{\partial}{\partial n}\left(\frac{u}{u_e}\right)\right]^2 dn \\
P &= \delta^*\left[\frac{\partial}{\partial n}\left(\frac{u}{u_e}\right)\right]_{n=0}
\end{aligned} \tag{8}$$

One profile shape parameter, say a(s), is chosen and the other profile quantities in Equation (8) will be determined as functions of it. Equations (4-6) can then be written:

$$\frac{d\delta^*}{ds} - \frac{Z\delta^*}{u_e}\frac{du_e}{ds} = \tan\Theta \tag{9}$$

$$H\frac{d\delta^*}{ds} + \frac{\delta^*}{u_e}(2H+1)\frac{du_e}{ds} + \delta^*\frac{dH}{da}\frac{da}{ds} = \frac{\nu P}{u_e\delta^*} \tag{10}$$

$$J\frac{d\delta^*}{ds} + \frac{3J\delta^*}{u_e}\frac{du_e}{ds} + \delta^*\frac{dJ}{dH}\frac{dH}{da}\frac{da}{ds} = \frac{\nu R}{u_e\delta^*} \tag{11}$$

The unknowns in these three ordinary differential equations are δ^*, u_e, Θ and a(s). This set of equations is known as the strong interaction equations when u_e is considered unknown. The outer inviscid flow is then coupled to the inner viscous flow.

The flowfield can be divided into four distinct regions in terms of the nature of the velocity profiles. They are illustrated in Figure 2. Region I, the body-attached flow region, extends from the leading edge to the separation point. Region II, the body-reverse flow region, extends from the separation point to the trailing edge. Region III, the wake-reverse flow region, extends from the trailing edge to the rear stagnation point of the wake. Region IV, the wake forward flow region, extends from the wake rear stagnation point to downstream infinity. Following Klineberg and Lees[6] and Klineberg, Kubota and Lees[12], a(s) is defined in the four regions as

Region I $\quad a = \left.\frac{\partial(u/u_e)}{\partial(n/\delta)}\right|_{n=0}$

Region II $\quad a = \left[\frac{n}{\delta}\right]_{u/u_e = 0}$

Region III $\quad a = \left[\frac{u}{u_e}\right]_{\psi=0}$

Region IV $\quad a = \left[\frac{u}{u_e}\right]_{n=0}$

a(s) is therefore the wall shear stress, the thickness of the reverse flow region and the velocity ratios on the dividing streamline $\psi = 0$ and the wake center line, respectively.

Similar solutions to the classical boundary-layer equations are available for profiles characteristic of each of the regions. It is assumed that the functional relationships between the profile quantities in Equation (8) and a(s) are the same as those for the similar solutions. It is noted, however, that no dependence between profile shape and local pressure gradient is assumed. Extensive curve fitting has led to accurate polynomial representation of the profile quantities as functions of a(s). These are presented in Appendix A for each region. The results for the profiles in regions I and II are those in Klineberg and Lees[6] and for profiles in regions III and IV are those in Klineberg, Kubota and Lees[12]. This choice of a(s) is made because of the availability of the above curve fits. A better choice might be H since it has one definition in the flowfield - Klineberg and Steger[8] use H in their analysis.

Boundary-layer theory predicts that tan θ, δ and δ^* are of order $\nu^{1/2}$. To work with variables of order one, the following scaling

is introduced.

$$(\tan\Theta)' = \nu^{-1/2} \tan\Theta$$
$$(\delta^*)' = \nu^{-1/2} \delta^* \qquad (13)$$
$$\delta' = \nu^{-1/2} \delta$$

The new variables are substituted into Equations (9-11) and the primes are dropped. To put the equations in a suitable form for numerical integration, Kramer's Rule is used to isolate the first derivatives. The equations become

$$\frac{d\delta^*}{ds} = \frac{D_1}{D}, \quad \frac{du_e}{ds} = \frac{D_2}{D}, \quad \frac{da}{ds} = \frac{D_3}{D} \qquad (14)$$

where

$$D_1 = \tan\Theta \left[(2H+1)\frac{dJ}{dH} - 3J\right] + Z\left(P\frac{dJ}{dH} - R\right)/u_e\delta^*$$

$$D_2 = \left(P\frac{dJ}{dH} - R\right)/\delta^{*2} - u_e \tan\Theta \left(H\frac{dJ}{dH} - J\right)/\delta^*$$

$$D_3 = [R(2H+1+ZH) - PJ(3+Z)]/\left(u_e\delta^{*2}\frac{dH}{da}\right) + J\tan\Theta\,(H-1)/\delta^*\frac{dH}{da}$$

$$D = \frac{dJ}{dH}(2H+1+ZH) - J(3+Z)$$

B. <u>The Interaction Equation</u>

There are now three viscous flow equations and four unknowns, one of them being u_e, the inviscid streamwise velocity component at the boundary-layer edge. It is necessary to introduce an equation to close the system and this equation is the important one which provides for

the interaction between the viscous boundary layer and the outer inviscid flow. For problems with a supersonic outer stream, a Prandtl-Meyer relation is usually used to link Θ and u_e. The problem becomes complicated in incompressible flow because the inviscid equations are elliptic and therefore global in nature. The local boundary-layer edge velocity depends on the displacement thickness distribution in the complete flow-field.

Consider the flow schematic shown in Figure 3 where U_∞ is the free stream speed. x and y are along and normal to the chordline. Let U and V be the velocity components in the x and y directions, respectively. With viscous effects included, the effective body shape is obtained by adding the displacement thickness to the body. Note that δ^* is measured normal to the body surface. Let $y = f(x)$ represent the body and let its geometry be such that thin-airfoil theory approximations are valid.

The effective body shape is represented by a distribution of sources along the x - axis of strength q(x) per unit length. The velocity potential for the irrotational flow is then

$$\phi(x,y) = U_\infty x + \frac{1}{2\pi} \int_0^\infty q(\xi) \log [(x-\xi)^2 + y^2]^{1/2} d\xi$$

where

$$q(x) = 2U_\infty \frac{d}{dx} [f(x) + \nu^{1/2} \delta^*/(1 + (\frac{df}{dx})^2)^{1/2}]$$

To the order of approximation of thin-airfoil theory, $(df/dx)^2 << 1$ and can be neglected in the above equation. Now,

$$U = \frac{\partial \phi}{\partial x} = U_\infty + \frac{U_\infty}{\pi} \int_0^\infty \left[\frac{df}{dx}(\xi) + \nu^{1/2} \frac{d\delta^*}{dx}(\xi)\right] \frac{x-\xi}{(x-\xi)^2+y^2} d\xi$$

$$V = \frac{\partial \phi}{\partial y} = \frac{U_\infty}{\pi} \int_0^\infty \left[\frac{df}{dx}(\xi) + \nu^{1/2} \frac{d\delta^*}{dx}(\xi)\right] \frac{y}{(x-\xi)^2+y^2} d\xi$$

and

$$\nu^{1/2} (\tan \theta)_{inviscid} = \frac{V(x, f+\nu^{1/2}\delta)}{U_\infty}$$

$$= \frac{1}{\pi} \int_0^\infty \left[\frac{df}{dx}(\xi) + \nu^{1/2} \frac{d\delta^*}{dx}(\xi)\right] \left[\frac{f(x)+\nu^{1/2}\delta(x)}{(x-\xi)^2+(f+\nu^{1/2}\delta)^2}\right] d\xi$$

Note that $(\tan \theta)_{inviscid}$ is measured with respect to x while $\tan \theta$ is measured with respect to s or the local body slope. Therefore,

$$\nu^{1/2} \tan \theta = \nu^{1/2} (\tan \theta)_{inviscid} - \frac{df}{dx}$$

and finally, the equation linking the flowfields is

$$\tan \theta = \frac{f(x)+\nu^{1/2}\delta(x)}{\pi} \int_0^\infty \left[\frac{df}{dx}(\xi) + \nu^{1/2} \frac{d\delta^*}{dx}(\xi)\right] \frac{d\xi}{(x-\xi)^2+(f+\nu^{1/2}\delta)^2}$$

$$- \nu^{-1/2} \frac{df(x)}{dx} \qquad (15)$$

C. Matching Conditions

For the viscous calculation, there are four distinct regions with different definitions of profile parameter a(s) and different polynomial relationships between the profile quantities. It is therefore necessary to enforce matching conditions as the solution progresses from one region into another. Physical considerations lead to the condition that displacement thickness δ^* and inviscid speed u_e are continuous across region boundaries.

Since a(s) is defined differently in each region, conditions on it are considered separately. In region I, a(s) is the wall shear stress and the region ends at the separation point a = 0. In region II, a is the thickness of the reverse flow region and a = 0 at the start of the region. In region III, a is the dividing streamline velocity ratio. At the trailing edge, let a(II) be the value in region II and a(III) be the value in region III. Klineberg, Kubota and Lees[12] have developed a curve fit for a(III) as a function of a(II) and it is used as the trailing edge matching condition.

$$a(III) = .05496\, a(II) + .29702\, a(II)^2 + 11.19943\, a(II)^3 - 21.66525\, a(II)^4 + 10.06854\, a(II)^5 \qquad (16)$$

At the end of region III, the wake rear stagnation point, a = 0. At the start of region IV, a is the wake centerline velocity ratio and is also zero.

D. Airfoil and Initial Potential Flow Solution

An airfoil must be selected such that separation will occur but also such that thin-airfoil approximations will be appropriate. A symmetric airfoil at zero angle of attack is chosen so that the difficulties involved with correctly determining the circulation do not add to the complexity of the problem. For ease in calculation of the initial potential flow, a Joukowski airfoil section is used.

Van Dyke[13] states that to second order a Joukowski airfoil is represented by

$$y = \varepsilon(2-x)(2x-x^2)^{1/2} \qquad (17)$$

where the chord is 2 and the maximum thickness ratio is $3^{3/2}\varepsilon/4$. For the 10% thickness ratio used in the analysis, $\varepsilon = .077$. The surface speed

u_e can easily be determined by use of conformal mapping. The Joukowski transformation maps the airfoil into a circular cylinder. To obtain $u_e(s)$, it is necessary to compute $s(x)$. The airfoil, its slope and surface speed are given in Figure 4.

Chapter III

METHODS OF SOLUTION

The mathematical problem to be solved is given in Equations (14) and (15) with the appropriate polynomial representations of the profile quantities (Appendix A) and the matching conditions. The Reynolds number considered is of the order of 10^4.

A. Karman-Pohlhausen on Airfoil Forward Portion

Initially, it was felt that the upstream influence of the separated flow region would be of limited extent. Therefore, the flow variables in the leading-edge portion of the airfoil would have the values predicted by classical boundary-layer theory. This assumption removes the need to use Equation (16), the linking equation, in the airfoil stagnation point region where the thin-airfoil approximations are invalid.

For ease of computation, the boundary-layer equations were integrated using the Karman-Pohlhausen method as described in Schlichting[14]. This integral method was chosen because it is accurate in regions of accelerated flow and also because the integral quantities it provides as output are just those needed in the interaction scheme. A more accurate finite-difference calculation could easily be used to replace the Karman-Pohlhausen scheme.

The Karman-Pohlhausen method was applied to the Joukowski airfoil with the previously calculated u_e distribution. The separation point was predicted at approximately s = .66S where S is the arclength of the airfoil. At tne stagnation point, the method yields

$$a = 3.192, \qquad \delta^* = .641/\frac{du_e}{ds}\Big|_{s=0}$$

It should be noted that the displacement thickness distribution agrees more closely with the finite-difference results than does the profile shape parameter a distribution.

To begin the computational procedure, an initial estimate for $\tan \Theta(s)$ is needed. Equation (15) shows that this requires initial estimates of the δ and δ^* distributions. Since the $\tan \Theta$ distribution will be continually updated in our interation procedure, a reasonable estimate is all that is necessary. The Karman-Pohlhausen results are used up to separation and then the estimates are guided by the experimental results of Preston and Sweeting[15]. For simplicity, the boundary layer thickness is assumed to increase linearly even though in the far wake it should become proportional to $s^{1/2}$. $\tan \Theta$ is much more sensitive to δ^* than to δ and some numerical experimentation was necessary to obtain a reasonable δ^* estimate. δ^* was assumed to increase linearly from the separation point to the trailing edge and then to follow the equation

$$\delta^* = 1 + 12(S/s)^{1/2}$$

in the wake which exhibits the proper asymptotic behavior in the far wake.

A description of the computational procedure is given below.

(1) $\tan \Theta(s)$ is calculated from Equation (15) using Simpson's Rule for the numerical integration. δ and δ^* are held fixed at their boundary-layer values for the first 15% of the arclength so that $\tan \Theta$ need only be calculated for $s \geq .15S$. The integration proceeds up to $s = 15S$ since integration further downstream did not appear to affect the results on the airfoil.

(2) Equations (14) are integrated numerically in the interval $.15S \leq s \leq 15S$ using a Runge-Kutta program from the University of Maryland Computer Science Center library. $\tan \theta$ is taken as the average value at the endpoints of each interval. At $s = .15S$, a, δ^* and u_e are taken from the Karman-Pohlhausen results. The integration yields updated values for δ, δ^*, a and u_e.

(3) The cycle is repeated with the newly calculated values of δ and δ^* being used in (1)

Far downstream, u_e should approach U_∞ and δ^* should approach a constant value. For a solution to be obtained the iteration procedure above must converge and be independent of the starting point for the strong interaction integration (taken arbitrarily above as .15S).

It is difficult to assess whether the above procedure has in fact converged. It would appear to depend to some extent on which variables are being monitored. A typical computation is demonstrated in Table 1 where the variables shown are the separation point location, a, δ^* and u_e at $s = 15S$ and δ^* at the airfoil trailing edge. The separation point moves closer to the airfoil leading edge with each iteration (eight iterations are recorded). The resulting solution is highly suspect since it seems unlikely that for the thin airfoil under consideration the separation point would occur so great a distance upstream of the value predicted by classical boundary-layer theory.

Some typical distributions of δ^*, u_e and $\tan \theta$ are shown in Figures (5-9) for three iteration cycles. Note that some of the variables

deviate immediately from the Karman-Pohlhausen results at the start of the strong interaction region. This is in violation of the assumption made regarding the limited upstream influence. Attempts to improve the convergence properties of the scheme by using under-relaxation in updating Equation (15) met with failure.

Solutions were attempted with the starting point taken further from the leading edge and when the strong interaction computations were begun for $s \geq .40S$, the scheme appeared to converge but the computed separation point proved to then be dependent on the starting point. For example, for starting points of .40S, .45S and .50S, the calculated separation points were .49S, .54S and .58S. This is clearly unacceptable. The results at the end of 10 iterations for the starting point of .50S are shown in Table 2.

B. Weak Interaction Equations in Airfoil Forward Portion

To be more consistent in the analysis, it is felt that the equations used in the forward portion of the airfoil should be the same as those used elsewhere. This should lead to smoother joining at the start of the strong interaction region. Consider the differential equations (9-11). In the leading-edge region, it is assumed that u_e is given from the potential flow solution. Equation (9) is now eliminated and Equations (10-11) will be integrated to obtain δ^* and a, using the known u_e distribution. This abbreviated set is known as the weak interaction equations.

δ, δ^* and $\tan \theta$ are again scaled with $\nu^{1/2}$ and the first derivatives are obtained in the form of Equations (14).

$$\frac{d\delta^*}{ds} = \frac{N_1}{N}, \quad \frac{da}{ds} = \frac{N_2}{N} \tag{18}$$

where

$$N_1 = \left[\left(P\frac{dJ}{dH} - R\right) + \delta^{*2}\frac{du_e}{ds}\left(3J - (2H+1)\frac{dJ}{dH}\right)\right]\left(\frac{dH}{da}/u_e\right)$$

$$N_2 = (RH-PJ)/\delta^* u_e + \delta^*\frac{du_e}{ds}\, J(1-H)/u_e$$

$$N = \delta^*\frac{dH}{da}\left(H\frac{dJ}{dH} - J\right)$$

The computational scheme now proceeds essentially the same as in Part A. The weak interaction equations are integrated from the leading edge to a point at the start of the strong interaction region, a distance far upstream of separation. This solution provides the starting values of δ^*, a and u_e for the strong interaction computation. The weak interaction equations predict separation at approximately 50% of the arclength so the initial estimates for δ and δ^* must be suitably modified.

Care must be taken in starting the weak interaction solution at the leading edge. Note that at the leading-edge stagnation point, both $\frac{d\delta^*}{ds}$ and $\frac{da}{ds}$ are proportional to u_e^{-1}. Since these derivatives must both be finite at s = 0, the following relationships can be obtained at s = 0 from Equations (18).

$$3PJ = R(2H+1) \tag{19}$$
$$\delta^{*2} = P/(2H+1)\left.\frac{du_e}{ds}\right|_{s=0}$$

The first expression leads to a = 2.967. The equations have a saddle point singularity at the leading edge. For the first .1% of the arclength, a similar solution is assumed so that a = 2.967 = constant. Equation (10) is integrated analytically from s = 0 to s = .001S using average values of u_e and du_e/ds in the interval. The result is

$$\frac{\delta^{*2}(.001S)}{\delta^{*2}(0)} = \left[2\frac{du_e}{ds}(0) + \left(\frac{du_e}{ds}(.001S) - \frac{du_e}{ds}(0)\right)e^{-\frac{2(2H+1)}{H}\left(\frac{1}{u_e}\frac{du_e}{ds}\right)_{avg}(.001S)}\right] \Big/ \frac{du_e}{ds}_{avg}$$

where avg stands for the average of the end point values. Equations (18) are numerically integrated downstream from s = .001S with care being taken to use small intervals in the leading-edge region. The weak interaction solutions for a and δ^* are compared to the Karman-Pohlhausen results in Figure 10.

The complete scheme was run with the strong interaction region starting at both 15% and 30% of the arclength. There is no appreciable difference from the results of Part A.

Another suggestion (Klineberg[16]) is to match the momentum thickness at the trailing edge rather than the velocity on the dividing streamline. Since $H = \theta/\delta^*$ and δ^* is continuous, this is equivalent to forcing H to be continuous at the trailing edge. In region III,

$$H = .24710 - .43642a - .04773a^2 - .19654a^3 + .41918a^4$$

At the trailing edge, H is known from its value in region II and a is determined from the above equation. Use of this matching condition had little effect on the results.

C. Velocity Dependent Interaction Equation

It has been suggested (Klineberg[16]) that the reason for the lack of success of the scheme is the possibility that Equation (15) and the integral continuity equation are not independent equations. Therefore, a new form of the equation linking the viscous and inviscid regions will be considered. It is obtained by a simple modification of the result given in Alber[7] for the incompressible wake.

Let $\bar{U}$ and $\bar{V}$ be the perturbation velocity components of the potential flow. Since they are harmonic conjugates, they are related by use of the Cauchy Integral Formula and the thin-airfoil approximation in the following equations.

$$\bar{U}(x,y) = \frac{1}{\pi}\int_{-\infty}^{\infty} \frac{y\bar{V}(\xi,0)}{(x-\xi)^2+y^2}\,d\xi$$

$$\bar{V}(x,y) = -\frac{1}{\pi}\int_{-\infty}^{\infty} \frac{(x-\xi)\bar{U}(\xi,0)}{(x-\xi)^2+y^2}\,d\xi$$

This representation is formally equivalent to representing the effective body by a vortex distribution on the chordline. Now,

$$U(x,y) = U_\infty + \bar{U}(x,y) \text{ and } \bar{U}/U_\infty << 1$$

Therefore,

$$(\tan\theta)_{\text{inviscid}} = \frac{\bar{V}(x, f(x)+\nu^{1/2}\delta(x))}{U_\infty}$$

$$= \frac{1}{\pi}\int_{-\infty}^{\infty} \frac{(x-\xi)[1-U(\xi,0)/U_\infty]}{(x-\xi)^2+(f+\nu^{1/2}\delta)^2}\,d\xi$$

On the surface, the limiting process of boundary-layer theory yields $U(\xi,0) = u_e(\xi)$. Using this and the previously developed relationship between $(\tan\theta)_{\text{inviscid}}$ and $\tan\theta$, the new form of the linking equation becomes

$$\tan\Theta = \frac{1}{\pi}\int_{-\infty}^{\infty} \frac{(x-\xi)[1-u_e(\xi)/U_\infty]}{(x-\xi)^2 + (f+\nu^{1/2}\delta)^2}\, d\xi \; - \; \nu^{1/2}\frac{df(x)}{dx} \qquad (20)$$

Note that $\tan\Theta$ now depends on u_e instead of δ^*.

To obtain an initial estimate for the $\tan\Theta$ distribution, several u_e distributions were tried but it proved difficult to choose a u_e distribution which would lead to a reasonable $\tan\Theta$. The next approach was to assume a $\tan\Theta$ distribution directly for the first iteration cycle.

It was possible to select $\tan\Theta$ distributions which led to apparently reasonable values of u_e and the other flow variables in the first iteration cycle but which yielded an unacceptable $\tan\Theta$ distribution for the second cycle. To demonstrate the sensitivity of the scheme, consider the two $\tan\Theta$ estimates.

$$\begin{aligned} \tan\Theta &= 5\sin\pi\, s/2S \qquad && s \le S \\ &= -2(S/s)^{3/2} && s > S \end{aligned} \qquad (21a)$$

and

$$\begin{aligned} \tan\Theta &= 6\sin\pi\, s/2S \qquad && s \le S \\ &= -2(S/s)^{3/2} && s > S \end{aligned} \qquad (21b)$$

The u_e distributions from the first iteration cycle are shown in Figure 11. The resulting $\tan\Theta$ distributions are shown in Figure 12. In Figure 13, the $\tan\Theta$ integral is separated into its airfoil and wake components. The term due to the airfoil slope is also shown. It can be seen that the major differences in the two cases stem from the wake contribution to the integral and that $\tan\Theta$ is very sensitive to the wake results. Note also that the airfoil slope term is dominant over a large portion of the airfoil. It is difficult to obtain a $\tan\Theta$ distribution

in the second cycle which is not negative for a substantial portion of the leading-edge region and this leads to unreasonable predictions from the viscous computation. With the above formulation, it was not possible to obtain reasonable results for more than two or three iteration cycles.

In the previous formulation of the linking equation, there is no contribution to the integral from the flowfield upstream of the leading edge. Equation (20), however, has a contribution from this region since $u_e \neq U_\infty$ in the upstream neighborhood of the leading edge. u_e was calculated from potential flow theory for $x < 0, y=0$. This portion of the u_e distribution is shown in Figure 14. Inclusion of these results improves the tan θ distribution on the airfoil but has a harmful effect in the wake region. tan θ with the upstream effect included is compared to the result with the latter initial estimate in Equation (21) in Figure 15.

At this time it was decided that the form of the linking equation given in Equation (20) was too sensitive to the flow quantities to be useful and that the most productive path to follow was to return to the formulation of Equation (15) and work towards developing a means to correctly update the solution in the leading edge region with each iteration cycle.

It is possible that the decision to abandon the formulation of the linking equation presented here was a mistake. In their successful treatment of a similar problem, Klineberg and Steger[8] also encountered difficulty in the initial iterations due to erroneous wake results.

Their fix was to initially choose the downstream boundary of their computation region to be close to the airfoil trailing edge and to gradually move it downstream as the calculations proceeded. Also, they used rather strong under-relaxation to improve the scheme's stability.

D. Updating of Solution in Airfoil Forward Portion

A major deficiency of the method as it has been used is that the weak interaction solution is fixed for the forward portion of the airfoil up to the joining point with the strong interaction region. The flowfield near the leading edge is not allowed to adjust to the downstream changes in the displacement thickness distribution. This enforces a certain dependence of the final solution on the choice of a joining point - it is not clear, however, whether this alone has prevented a solution from being obtained.

It is necessary to develop a method to calculate the potential flow surface speed for the flow past body plus displacement thickness which is more accurate than first-order thin-airfoil theory in the important leading-edge region. This method must be computationally easy to use or the purpose of originally using the thin-airfoil approximations will be defeated. Von Karman[17] had developed such a method for the solution for the potential flow past axisymmetric bodies. The method has been modified here for use in the two-dimensional case.

The airfoil chordline is divided into constant length intervals and a source distribution is introduced with the source strength being

constant for each interval. It is therefore necessary to calculate a finite number of source strengths. A major cause of error in the thin-airfoil approach is caused by the linearization and the transfer of the body boundary condition to the chordline. Both of these deficiencies are overcome in Von Karman's method since the exact boundary condition is used and it is satisfied on the actual surface. The boundary condition is satisfied at the surface points corresponding to the midponts of the constant source intervals. The result is a set of linear equations for the unknown source strengths which is solved numerically.

The details of the method are described in Appendix B. A comparison of the results for the Joukowski airfoil with the exact solution and the first-order thin-airfoil result for surface speed is given in Figure 16. Agreement with the exact solution is very good for distances greater than about .03S from the leading edge. The smallest constant source interval that could be used without introducing fluctuations into the surface speed was .01c where c is the chord length.

This potential flow method is now incorporated into the computational scheme. To insure continuity from iteration to iteration, the results for the airfoil itself were used in the first iteration cycle. The scheme proceeds as before except that at the start of each cycle, the potential flow past the body plus its displacement thickness from the previous cycle is computed and the weak interaction equations are integrated to provide the joining values at the start of the strong interaction region. The effective body is terminated at the now open trailing edge -

this is consistent with current techniques for "exactly" calculating the flow past two-dimensional bodies with displacement thickness added (see, for example, Stevens, Goradia and Braden[18], where the effective airfoil is terminated closely behind the trailing edge). When the displacement thickness is added, the smallest source interval that can be used without smoothing the results is approximately .02c.

The results of three iteration cycles are shown in Figures 17-20. The effective body after one cycle is shown in Figure 17. The displacement thickness distribution is given in Figure 18 and u_e is given in Figures 19 and 20, the former showing the very small change in the surface speed in the leading-edge region from the first to the second iteration. The addition of the updating of the leading-edge portion of the flowfield does not appear to appreciably affect the results. The trend is indicated in Table 3. An acceptable solution still cannot be obtained.

As a final note, another deficiency of the method is discussed. For the strong interaction region, tan θ is calculated from the linking integral equation and used as input in the integral continuity equation. This continuity equation is not satisfied in the weak interaction region. The question arises, in consideration of the smoothness of the joining, as to the value of tan θ that is computed at the joining point by use of the continuity equation. For the previous set of computations, tan θ was calculated at the joining point from both equations and the comparison appears in Table 4. It is noted that the discrepancy between the values is less than 10%.

CHAPTER IV

SOLUTION OF KLINEBERG AND STEGER

Klineberg and Steger[8] have obtained solutions for subsonic and transonic separated flow past circular arc airfoils. The main difference between their computational technique and the one reported here is that they obtain a solution for the complete inviscid flowfield by use of a finite-difference relaxation scheme. Their method will now be described in the context of the previously reported procedures.

A. Viscous Flow

The system of equations which describes the flow in the viscous layer is the compressible flow equivalent to Equations (9-11). The four unknowns are chosen to be u_e, v_e, δ^* and H where v_e is used instead of tan Θ and H is chosen as the profile shape parameter.

The flow over the airfoil is divided into weak and strong interaction regions. In the weak interaction region, u_e is obtained from the inviscid flow calculation and the equivalent of Equations (10-11) are solved by Runge-Kutta integration. The equivalent of Equation (9) is then integrated to obtain v_e. A similarity solution is used to start the calculation at the leading edge. In the strong interaction region, v_e is given from the inviscid calculation and δ^*, H and u_e at the joining point are given from the weak interaction solution. δ^*, u_e and H are taken to be continuous at the boundaries of the four distinct profile regions.

B. Inviscid Flow

The flowfield outside the viscous region is considered to be irrotational and the transonic small disturbance approximation and

thin-airfoil boundary conditions are assumed. The governing partial differential equations are the continuity equation and the statement of the irrotationality of the flow in terms of the velocity components. Mixed boundary conditions are specified since the viscous computation yields v_e in the weak interaction region and u_e in the strong interaction region. Figure 21 shows a map of the flow regions. The equations are solved using the finite-difference relaxation scheme described in Steger and Klineberg[9].

C. Complete Interaction

A complete interaction is calculated by alternately iterating the solutions to the viscous and inviscid equations. The sequence of computations is described as follows:

(1) Solve the inviscid equations for the given airfoil. Compute the surface pressure distribution.

(2) Solve the weak interaction equations from the leading edge to the joining point. For the biconvex airfoils used, the joining point is chosen upstream of the maximum thickness location at 40% of the chord.

(3) Integrate the continuity equation to obtain v_e. Downstream of the joining point, v_e is arbitrarily specified in the first iteration cycle.

(4) Integrate the strong interaction equations using the assumed v_e. Compute the u_e distribution.

(5) Solve the inviscid equations with the mixed boundary conditions corresponding to v_e in the weak interaction region and u_e in the strong interaction region. Compute u_e in the weak interaction region and v_e in the strong interaction region.

(6) Alternate between viscous and inviscid solutions until convergence is achieved. The boundary conditions for the current viscous/inviscid computation are provided by the previous inviscid/viscous computation.

It is noted that the viscous and inviscid problems are linked through the surface speed in the strong interaction region. This technique is therefore related to the attempt to use Equation (20) as the linking equation in the previously reported research. It is recalled that this attempt was abandoned due to the sensitivity of the scheme to the flow variables in the initial stages of the computation.

It is perhaps significant that Klineberg and Steger encountered similar difficulties. Until their scheme converges to a solution, the viscous layer integration diverges in the wake and generates unacceptable values of u_e for use as boundary conditions for the inviscid problem. This difficulty is resolved in two ways. First, the location of the downstream boundary of the computation region is chosen close to the trailing edge initially and is moved downstream as the scheme progresses. Second, under-relaxation is employed in updating the inviscid flow boundary conditions in the wake. The above solution is aided by the use of an interactive computer graphics system. The discrepancy in $\tan \Theta$ at the joining point that was inherent in the previous research is absent from the Klineberg and Steger technique since the continuity equation supplies $\tan \Theta$ for the inviscid flow computation in the weak interaction region.

Results were obtained for a range of Reynolds numbers and Mach numbers for 6% and 12% thick biconvex airfoils. The results are independent of the initially chosen v_e distribution and joining point location. For some cases, an approximation to simulate a turbulent wake was included.

A typical solution is shown in Figure 22 to illustrate the distributions of u_e, δ^* and H. M_∞ is the free stream Mach number, Re_c is the chord Reynolds number, SEP indicates the separation point and RSP indicates the wake rear stagnation point. The final downstream boundary is located only 2.5 chordlengths downstream of the trailing edge. It is noted that previously the calculated distributions did not appear to approach asymptotic downstream values until much further downstream.

Comparison with the experimental results of Collins (unpublished) is shown in Figure 23. Agreement is good when the turbulent wake approximation is used. The effects of Reynolds number and Mach number are demonstrated in Figures 24 and 25. In these figures, C_p is the pressure coefficient.

CHAPTER V

CURRENT RESEARCH IN VISCOUS-INVISCID INTERACTIONS

At present, much work is being done in the area of viscous-inviscid interactions in flowfields with separation present. Research teams at various government, university and industrial laboratories are studying problems where the free stream is subsonic, transonic, supersonic and hypersonic, laminar and turbulent, and where the governing equations considered are either some form of the boundary-layer equations or the complete Navier-Stokes equations. In this chapter, an attempt is made to survey the current state-of-the-art and to essentially present a preview of what can be expected to appear in the literature in the next few years. This survey is by no means all inclusive.

The only solution to a subsonic interaction problem including separation to appear in the literature apparently is the solution of Klineberg and Steger[8] of NASA-Ames Research Center which is discussed in detail in Chapter IV. Their method employs an integral form of the boundary-layer equations and uses a finite-difference relaxation technique to solve for the inviscid flowfield. Due to the computational difficulties encountered in using the integral approach in the viscous region, no attempt has been made to extend the results. Klineberg is currently studying under what conditions regular solutions to the boundary-layer equations which admit regions of separated flow exist. Armed with this information, the group at Ames may again attack subsonic and transonic interaction problems using finite-difference techniques

in the viscous as well as the inviscid region.

A finite-difference technique to integrate the boundary-layer equations through regions of reverse flow is presented in Erdos, Baronti and Elzweig[11] in connection with a study of transonic viscous flow with interaction. The authors question whether a solution of the direct problem (airfoil geometry given) by an iteration process between the solutions in the viscous and inviscid regions will converge and therefore treat the indirect problem. The airfoil contour is specified over the forward portion of the chord and the pressure distribution over the rearward portion. The inviscid flowfield is obtained by a finite-difference relaxation of the transonic small disturbance equation. The viscous equations are integrated using a Crank-Nicholson type implicit finite difference technique. In regions containing reverse flow, the parabolic equations take on an elliptic-like character since the solution at a point depends on downstream information. This is accounted for by use of upwind differencing in the reverse flow region.

The viscous flow solution technique is verified by a solution for the incompressible flow past an elliptic cylinder using the measured pressure distribution as input. The theoretical results agree well with those from the experiment. The inviscid and viscous region solutions are not obtained simultaneously in this paper to generate a solution to the transonic interaction problem.

The method presented in the above paper has not been extended by the authors who are at Advanced Technology Laboratories. Instead, interest

has been generated in the more practical turbulent transonic interaction problem. Baronti is currently working in this area and has developed an integral technique for the integration of the equations in the turbulent viscous region. An integral form of the turbulent kinetic energy equation is used to take account of the history of the boundary layer. The energy equation and the mean equation of motion describe the flow in the viscous region. The inviscid flowfield is handled by a finite-difference scheme which integrates the transonic small disturbance equation. The viscous region and inviscid region equations have not yet been integrated simultaneously so that a solution is not now available. Baronti is presently considering the solution of the indirect problem.

Another group which is studying transonic interactions is led by R. Melnik of Grumman. The second-order accurate, implicit finite-difference scheme of Keller[19] is used to integrate the viscous equations. The boundary-layer equations are written as a set of first-order partial differential equations. Central differences are used in the streamwise direction to yield a block tri-diagonal system. To eliminate the pressure, the normal derivative of the streamwise momentum equation is used. This increases the order of the system and requires an extra boundary condition. This condition is obtained by a combination of the pressure-displacement thickness relationship at the viscous-layer edge and the wall compatibility condition which relates the pressure gradient to the normal wall shear stress gradient. Extrapolation is used in applying this condition.

The method is used to study transonic free interactions. An asymptotic linearized solution is introduced at upstream infinity and

the system of equations is integrated downstream. The integration marches into the reverse flow region before numerical instability occurs. To obtain a solution for larger downstream distances, one can use upwind differencing as suggested above by Erdos et al[11] or one can proceed as in Reyhner and Flugge-Lotz[20] and eliminate the convective acceleration term in the reverse flow region. Currently, Melnik is developing an asymptotic solution valid in the flowfield far downstream in the reverse flow region to determine the proper downstream condition which the unique solution must approach.

Melnik is also currently studying the subsonic (incompressible) interaction that occurs in the neighborhood of the trailing edge of a finite flat plate aligned parallel to a uniform stream. The above finite-difference technique is being used to integrate the boundary-layer type equations developed by Stewartson[21] for the inner viscous layer. The interaction proceeds as follows. First, the displacement thickness is prescribed and the boundary-layer equations are integrated and the pressure determined. The interaction equation relates the pressure to the displacement thickness in terms of a Cauchy integral and it is inverted to obtain an updated value of the displacement thickness. The cycle is then repeated. Upon the successful completion of this study, the angle of attack case will be considered.

Also, Melnik is attempting to extend the approach of Stewartson to the turbulent interaction problem. He feels that two-dimensional and axisymmetric laminar and turbulent interactions can be handled by use of finite-difference techniques coupled with a careful analysis of the asymptotic behavior of the solution.

M. Werle and co-workers at the University of Cincinnati and the

Aerospace Research Laboratories have been studying supersonic and hypersonic interactions. The method for solving the laminar, two-dimensional supersonic interaction problem is described in Werle, Polak and Bertke[22]. An implicit finite-difference scheme is used in the viscous flow region. The governing equations are the boundary-layer equations with interaction. An analytical justification for use of this model is given by Stewartson and Williams[23] who performed an asymptotic analysis of the compressible Navier-Stokes equations for supersonic flow over a flat plate. The numerical technique is similar to that of Reyhner and Flugge-Lotz[20] but the equations are written in Levy-Lees type variables. In the region of reverse flow, at points with negative streamwise velocity the convective acceleration term which induces numerical instability is set equal to zero. If a major portion of the viscous layer has reverse flow, it is necessary to introduce artificially positive convective terms. A key to the success of the technique is the control of the continuity equation and its coupling to the momentum equation. The continuity equation is integrated from the viscous-layer edge to the wall and iteration is necessary to correct the assumed value of the edge normal velocity component.

The interaction model makes use of linear theory to relate the pressure to the inviscid streamline deflection angle for the flow past the body plus its displacement thickness. The system is solved as follows. The problem is an initial value one and a "shooting" approach is used to correctly satisfy the downstream boundary condition. Self-

similar solutions are used at the upstream station. The energy equation is integrated using assumed profiles. The momentum and continuity equations are then integrated. The interaction equation is used to update the edge conditions and the cycle is repeated. Recently, Werle has developed a relaxation scheme to satisfy the downstream boundary condition which significantly reduces computation time.

Results for the free interaction problem agree well with those of Stewartson and Williams[23]. Reasonable results are obtained for flows with shock-wave and ramp-induced separation bubbles when the inverse problem is considered.

The hypersonic interaction problem is treated in Dwoyer[24]. Werle, Vatsa and Bertke[25] have taken a step towards solution of the three-dimensional interaction problem by solving for the flow past a swept compression ramp in a Mach 3 stream. The three-dimensional boundary-layer equations with constant cross flow are solved in Levy-Lees type variables. Linearized theory is used to relate boundary-layer growth to displacement surface angle. The solution technique follows that of the two-dimensional case.

L. Olson and R. MacCormack of NASA-Ames Research Center are currently studying the solution of laminar subsonic interactions by the numerical integration of the Navier-Stokes equations. The method used is the time-dependent finite-difference technique of MacCormack[26]. To test the method for subsonic viscous flows, solutions have been obtained for flow into an inlet and flow past a flat plate cascade with Reynolds number based on channel width varying from approximately 20 to 150. A paper

is in preparation in which comparisons are made with existing incompressible steady state solutions.

At present, they are studying the subsonic interaction in the trailing-edge region of a finite flat plate aligned parallel to the stream. The Reynolds number is of the order of 100 and the Mach number is less than .4. Upon the successful completion of this endeavor, many avenues of extension are open. Apparently, the next step will be to consider adding a turbulence model to the flat-plate interaction. It is felt that at present the cost of exploring high Reynolds number solutions is prohibitive.

CHAPTER VI

DISCUSSION AND CONCLUSIONS

This report describes a method proposed to treat the problem of steady, two-dimensional, laminar, incompressible, high Reynolds number separated flow past thin airfoils. An integral description of the flowfield in the viscous region is used and the interaction between the inviscid and viscous flowfields is provided for by use of a thin-airfoil integral. In the light of the failure of this method to generate a solution, it is useful to compare it with the methods discussed in Chapters IV and V to help explain the lack of success and to suggest the path that future research might follow.

Solutions to this or related problems with large Reynolds number by means of numerical solution of the Navier-Stokes equations are not available at present and do not appear to be forthcoming in the near future. This is unfortunate since these "exact" solutions could be used to test the validity of the approximate model equations which have been proposed. The methods discussed here use the boundary-layer equations with interaction to describe the flow in the viscous region. Some justification of this model for a supersonic mainstream and self-induced separation is given in Stewartson and Williams[23] but the asymptotic limit as Reynolds number goes to infinity is considered. The subsonic interaction is on even less of a firm footing since the most extensive research has been on the interaction at the trailing edge of a flat plate, a case without separation or reverse flow. It is clear that the need exists to provide further justification for the use of boundary-layer equations to study separated flow.

In the viscous flow region, either an integral or a finite-difference representation is used. In the pioneering work of Lees and co-workers, use of the integral form was motivated by the complexity of the computation and the absence of a suitable finite-difference scheme. According to Melnik and Werle, schemes to integrate into reverse flow regions are well in hand and it no longer appears to be necessary to use the integral approach.

For the inviscid flow computation, two alternatives also exist. Most researchers consider a linearized interaction where the flow deflection angle or pressure is related to the slope of the displacement thickness. Klineberg and Steger and Baronti use a finite-difference integration for the inviscid region - this provides for a conceptually more direct matching at the viscous-layer edge.

The method described here is somewhat unique. In the viscous region, the approach of Klineberg and Steger[8] is followed. However, in the inviscid region, the approach is similar to the integral representation of Melnik. This may be where the difficulty arises. The approach is the only one to use both the integral continuity equation and the flow angle-displacement thickness slope integral simultaneously. The equations have the same form and may not provide independent information.

The major difficulty encountered in the use of an integral form of the linking equation, either the description given in IIB or the one in IIIC, for the subsonic interaction case with separation is the need to update the inviscid flowfield in the forward portion of the airfoil. This requires an auxiliary inviscid computation and negates to some extent the simplicity achieved by using an integral approach in the first place. For this reason, it appears that at the present time the most

effective way to handle the solution of the inviscid region equations is with a finite-difference relaxation scheme. It would be useful in treating a more general body to eliminate the "small disturbance" limitations of some of the current schemes. The essential features of the flow in the viscous region are captured by the use of an integral approach however increased accuracy of the solution and an improved knowledge of the details of the flowfield can be obtained by the use of a finite-difference technique in this region.

In summary, a technique is not yet available for the solution of subsonic viscous-inviscid interactions with separation although much research is currently in progress. It is recommended that finite-difference schemes be used to calculate the flowfields in both the viscous and inviscid regions.

References

1. Van Dyke, M., "Higher-Order Boundary-Layer Theory," Annual Review of Fluid Mechanics, Vol. 1, Annual Reviews Inc., Palo Alto, California, 1969, pp. 265-292.
2. Davis, R.T., "Numerical Solution of the Navier-Stokes Equations for Symmetric Laminar Incompressible Flow Past a Parabola," Journal of Fluid Mechanics, Vol. 51, Part 3, 1972, pp. 417-433.
3. Davis, R.T., and Werle, M.J., "Numerical Solutions for Laminar Incompressible Flow Past a Paraboloid of Revolution," AIAA Journal, Vol. 10, No. 9, 1972, pp. 1224-1230.
4. Jacob, K., "Calculation of Incompressible Separated Flow Around Lifting Airfoils and Calculation of Maximum Lift," Zeitschrift fur Flugwissenschaften, Vol. 17, No. 7, 1969, pp. 221-230.
5. Bluston, H.S., and Paulson, R.W., "A Theoretical Solution for Laminar Flow Past a Bluff Body with a Separated Wake", Journal de Mecanique, Vol. 11, No. 1, 1972, pp. 161-180.
6. Klineberg, J.M., and Lees, L., "Theory of Laminar Viscous-Inviscid Interactions in Supersonic Flow," AIAA Journal, Vol. 7, No. 12, 1969, pp. 2211-2221.
7. Alber, I.E., "Integral Theory for Turbulent Base Flows at Subsonic and Supersonic Speeds," Ph.D. thesis, California Institute of Technology, 1967.
8. Klineberg, J.M., and Steger, J.L., "Calculation of Separated Flows at Subsonic and Transonic Speeds," Presented at the Third International Conference on Numerical Methods in Fluid Dynamics, Paris, France, July 3-7, 1972.

9. Steger, J.L., and Klineberg, J.M., "A Finite-Difference Method for Transonic Airfoil Design," AIAA Journal, Vol. 11, No. 5, 1973, pp. 628-635.

10. Klemp, J.B., and Acrivos, A., "A Method for Integrating the Boundary-Layer Equations Through a Region of Reverse Flow," Journal of Fluid Mechanics, Vol. 53, Part I, 1972, pp. 177-191.

11. Erdos, J., Baronti, P. and Elzweig, S., "Transonic Viscous Flow Around Lifting Two-Dimensional Airfoils," AIAA Paper No. 72-678, 1972.

12. Klineberg, J.M., Kubota, T. and Lees, L., "Theory of Exhaust-Plume/ Boundary-Layer Interactions at Supersonic Speeds," AIAA Journal, Vol. 10, No. 5, 1972, pp. 581-588.

13. Van Dyke, M., Perturbation Methods in Fluid Mechanics, Academic Press, New York, 1964, p. 54.

14. Schlichting, H., Boundary-Layer Theory, McGraw Hill, New York, Sixth Edition, 1968, p. 192.

15. Preston, J.H., and Sweeting, N.E., "The Experimental Determination of the Boundary Layer and Wake Characteristics of a Simple Joukowski Airfoil, with Particular Reference to the Trailing Edge Region," R and M 1998, 1943.

16. Klineberg, J.M. (Private Communication)

17. von Karman, T., "Calculation of Pressure Distributions on Airship Hulls," NACA Techn. Memo 574, 1930.

18. Stevens, W.A., Goradia, S.H., and Braden, J.A., "Mathematical Model for Two-Dimensional Multi-Component Airfoils in Viscous Flow," AIAA Paper No. 72-2, 1972.

19. Keller, H.B., and Cebeci, T., "Accurate Numerical Methods for Boundary-Layer Flows - I. Two Dimensional Laminar Flows," Proceedings of Second International Conference on Numerical Methods in Fluid Dynamics , Springer-Verlag, Berline, 1971

20. Reyhner, T.A., and Flugge-Lotz, I., "The Interaction of a Shock Wave With a Laminar Boundary Layer," Report No. 163, Division of Engineering Mechanics, Stanford University, California, 1966.

21. Stewartson, K., "On the Flow Near the Trailing Edge of a Flat Plate II," Mathematika, Vol. 16, 1969, pp. 106-121.

22. Werle, M.J., Polak, A., and Bertke, S.D., "Supersonic Boundary-Layer Separation and Reattachment - Finite Difference Solutions," Report No. AFL 72-12-1, University of Cincinnati, Aerospace Engineering Department, 1973.

23. Stewartson, K., and Williams, P.G., "Self-Induced Separation," Proceedings of the Royal Society of London, Ser. A, Vol. 312, 1969, pp. 181-206.

24. Dwoyer, D.L., "Supersonic and Hypersonic Two Dimensional Laminar Flow Over a Compression Corner," to be presented at the AIAA Computational Fluid Dynamics Conference, Palm Springs, California, July 1973.

25. Werle, M.J., Vatsa, V.N., and Bertke, S.D., "Sweep Effects on Supersonic Separated Flows - A Numerical Study," to be published in the AIAA Journal.

26. MacCormack, R.W., "Numerical Solution of the Interaction of a Shock Wave with a Laminar Boundary Layer," Lecture Notes in Physics, Vol. 8, 1971.

TABLE 1

A Typical Computation for the Method of IIIA

Iteration Number	Separation Point	a	At s = 15S u_e	δ^*	δ^* at Trailing edge
1	.47S	.685	.839	6.93	16.0
2	.38S	.706	.860	6.28	17.4
3	.34S	.715	.877	5.97	18.8
4	.31S	.718	.890	5.82	20.2
5	.30S	.719	.898	5.75	21.5
6	.29S	.719	.906	5.69	22.7
7	.28S	.719	.913	5.67	23.8
8	.27S	.718	.921	5.67	24.7

Note: The starting point is s = .15S

TABLE 2

Computation for the Method of IIIA with Starting Point at .50S

Iteration Number	Separation Point	a	At s = .15S u_e	δ^*	δ^* at Trailing edge
1	.62S	.722	.856	5.96	14.5
2	.60S	.768	.898	4.73	14.4
3	.59S	.795	.926	4.07	14.4
4	.58S	.810	.946	3.71	14.4
5	.58S	.819	.958	3.49	14.4
6	.58S	.825	.966	3.37	14.4
7	.58S	.829	.971	3.28	14.4
8	.58S	.832	.974	3.22	14.4
9	.58S	.834	.973	3.16	14.4
10	.58S	.837	.975	3.11	14.4

TABLE 3

A Typical Computation for the Method of IIID

Iteration Number	Separation Point	a	At s = 15S_* u_e	δ	δ^* at Trailing edge
1	.42S	.668	.850	5.16	10.7
2	.38S	.703	.883	4.42	11.2
3	.36S	.723	.903	4.03	11.7

Note: The starting point is s = .15S

TABLE 4

A Comparison of tan Θ at the Joining Point Calculated from the Continuity and Linking Equations

Iteration Number	tan Θ from Equation (9), Integral Continuity Equation	tan Θ from Equation (15), Linking Equation
1	2.043	2.019
2	2.344	2.125
3	2.492	2.297

Note: The computation is the same one used in Table 3.

APPENDIX A: POLYNOMIAL CURVE FITS OF PROFILE QUANTITIES

Table A1

Coefficients of Functions $F = \sum_{k=0}^{7} C_k a^k$ for Regions I, II, III

F	C_0	C_1	C_2	C_3	C_4	C_5	C_6	C_7
Region I								
H	0.24711	0.11056	-0.02122	0.00435	-0.00097	0.000099		
J	0.37372	0.16969	-0.02336	0.00572	-0.00175	0.000191		
Z	1.03539	0.48373	-0.01502	0.02610	-0.00370			
R	1.25782	-0.55550	0.31964	-0.09077	0.01398	-0.000935		
P		0.48745	-0.09927	0.00960	-0.00031			
dH/dA	0.11056	-0.04245	0.01304	-0.00389	0.00050			
dJ/dH	1.50031	0.28105	-0.04287	0.00262				
Region II								
H	0.24711	-0.25057	-0.43012	0.1430	-0.4267	-10.8587	38.7425	-31.209
J	0.37372	-0.42859	0.33036	-5.1517	10.5964	- 5.8174		
Z	1.03539	-1.02605	-1.12405	-1.1456	3.3434			
R	1.25782	1.09088	7.01736	-33.8762	196.7688	-371.9762	244.3095	
P		-1.19450	-0.70990	-7.1253	20.8568	-100.2729	310.2394	-263.587
dH/dA	-0.25057	-0.86024	0.42888	-1.7068	-54.2937	232.4553	-218.4664	
dJ/dH	1.50031	-0.84045	3.32376	-13.8668	5.4767	30.1770		
Region III								
H	0.24710	-0.43642	-0.04773	-0.19654	0.41918			
J	0.37368	-0.59326	-0.00220	0.27426	-0.39421			
Z	1.03285	-1.35026	0.05127	0.84914	-1.89847			
R	1.25775	2.02922	3.88529	-9.20873	16.34366			

dH/dA and dJ/da are obtained by differentiating the expressions for H and J, respectively. Then, dJ/dH = dJ/da/dH/da

In Region IV, the following curve fits apply.

$$\tilde{\delta} = 2.35860 - 5.27379a + 6.73235a^2 - 6.12945a^3 + 2.34196a^4$$

$$\tilde{H} = .58530 + .59289a - 2.14390a^2 + 1.48259a^3 - .52313a^4$$

$$\tilde{J} = .88674 + .67519a - 1.66397a^2 + .28925a^3 - .19051a^4$$

$$\tilde{Z} = 2.43208 + .98139a - .91905a^2 + 1.01789a^3 - .52020a^4$$

$$\tilde{R} = .53431 - .58670a - .62596a^2 + .89792a^3 - .22179a^4$$

The profile quantities are

$$H = \tilde{H}/\tilde{\delta}, \quad J = \tilde{J}/\tilde{\delta}, \quad Z = \tilde{Z}/\tilde{\delta}, \quad R = \tilde{R}\tilde{\delta}$$

Also,

$$\frac{dH}{da} = \frac{\tilde{\delta}\, d\tilde{H}/da - \tilde{H}\, d\tilde{\delta}/da}{\tilde{\delta}^2}$$

$$\frac{dJ}{da} = \frac{\tilde{\delta} d\tilde{J}/da - \tilde{J}\, d\tilde{\delta}/da}{\tilde{\delta}^2}$$

and

$$\frac{dJ}{dH} = dJ/da/dH/da$$

APPENDIX B: VON KARMAN POTENTIAL FLOW METHOD

Consider the potential flow of a uniform stream of speed U_∞ past a two-dimensional symmetric body given by the equation $y = f(x)$. The disturbance caused by the body will be represented by N source elements placed along the chordline (x-axis), each with constant strength over an interval of length Δx. The source with strength q_i per unit length lies in the interval extending from x_i to x_{i+1}. The velocity components of the flow induced by N of these sources at the point (x,y) are

$$\bar{U}(x,y) = \sum_{1}^{N} \frac{q_i}{4\pi} \log \frac{y^2 + (x-x_i)^2}{y^2 + (x-x_{i+1})^2} \tag{B1}$$

$$\bar{V}(x,y) = \sum_{1}^{N} \frac{q_i}{2\pi} \left(\tan^{-1} \frac{y}{x-x_{i+1}} - \tan^{-1} \frac{y}{x-x_i}\right)$$

The exact surface boundary condition is given by

$$\frac{\bar{V}(x,f(x))}{U_\infty+\bar{U}(x,f(x))} = \frac{df}{dx} \tag{B2}$$

If the boundary condition is satisfied at N surface points $(x_k, y_k = f(x_k))$, substitution of Equation (B1) into Equation (B2) leads, after some manipulation, to the equations

$$\sum_{i=1}^{N} A_{ik} Q_i = -\frac{df}{dx}(x_k) \qquad k = 1,2,3.....N \tag{B3}$$

where

$$Q_i = q_i/2U_\infty\pi$$

and

$$A_{ik} = \tan^{-1} \frac{y_k}{x_k-x_i} - \tan^{-1} \frac{y_k}{x_k-x_{i+1}} + \frac{1}{2} \frac{df}{dx}(x_k) \log \frac{y_k^2 + (x_k-x_i)^2}{y_k^2 + (x_k-x_{i+1})^2}$$

Equation (B3) is a set of N linear equations for the N unknown values of the normalized source strength Q_i. The equations can be put in matrix form and solved by a variety of techniques. Here they were solved by the Gauss-Jordan elimination method program from the University of Maryland Computer Science Center Library.

Once the Q_i's are obtained, the surface speed on the body can be computed. The components of velocity on the surface, U_k and V_k, are determined with the help of Equation (B1) and after some manipulation become

$$U_k = U_\infty + \sum_{i=1}^{N} \frac{U_\infty Q_i}{2} \log \frac{y_k^2 + (x_k - x_i)^2}{y_k^2 + (x_k - x_{i+1})^2} \tag{B4}$$

$$V_k = \sum_{i=1}^{N} U_\infty Q_i \cos^{-1}\left[\frac{(x_k-x_i)(x_k-x_{i+1}) + y_k^2}{[(x_k-x_i)^2+y_k^2]^{1/2}\,[(x_k-x_{i+1})^2+ y_k^2]^{1/2}}\right]$$

The surface speed is

$$u_e(x_k) = (U_k^2 + V_k^2)^{1/2} \tag{B5}$$

For the Joukowski airfoil, the equation of the surface is

$$y_k = \varepsilon(2-x_k)(2x_k-x_k^2)^{1/2}$$

One would expect that the accuracy of the solution would increase with the increase in the number of constant source intervals. This is true; however, there is a limit on the number of intervals that can be used for a particular geometry. For a 10% Joukowski airfoil, the maximum number of intervals possible was approximately 100. When the number was increased beyond this, oscillations appeared in the singularity distribution and in the resulting surface speed.

There is not complete freedom in the choice of the endpoints of the singularity distribution. For a closed airfoil, at the leading

and trailing edges $y_k = 0$. To compute the surface speed at the leading edge, $x_k = y_k = 0$ must be substituted into Equations (B4) and it is clear that if the singularity distribution begins at the airfoil leading edge and therefore $x_i = 0$, U_k becomes unbounded. For a particular geometry, there is a limitation in the distance between the leading edge and the start of the singularity distribution. For the 10% Joukowski airfoil, this distance was .5% of the chord. Starting the distribution any closer to the leading edge caused large oscillations in the surface speed in the leading-edge region.

The boundary conditions are satisfied at the surface points corresponding to the midpoints of the source elements. The following placement of the surface points x_k and the singularity points x_i is chosen.

$$x_k = k\Delta x$$

$$x_i = (i-1/2)\Delta x$$

For the 10% Joukowski airfoil, $x = .01c$ is chosen so that the first source element begins at $x = .005c$.

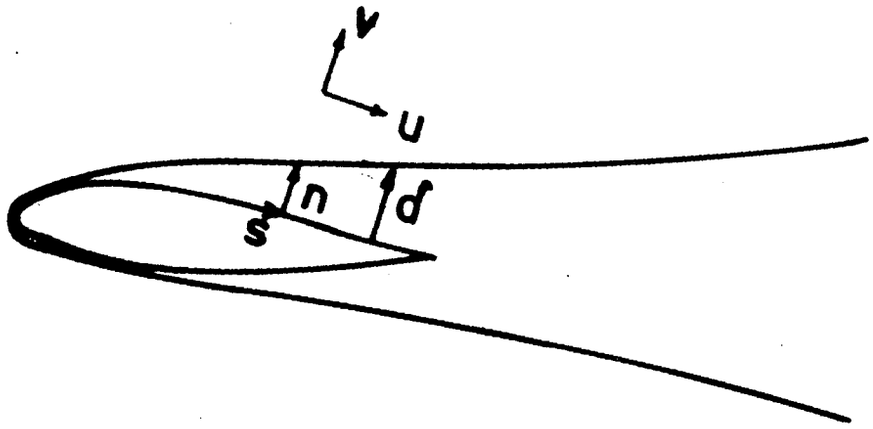

Figure 1. Coordinate System for Viscous Region

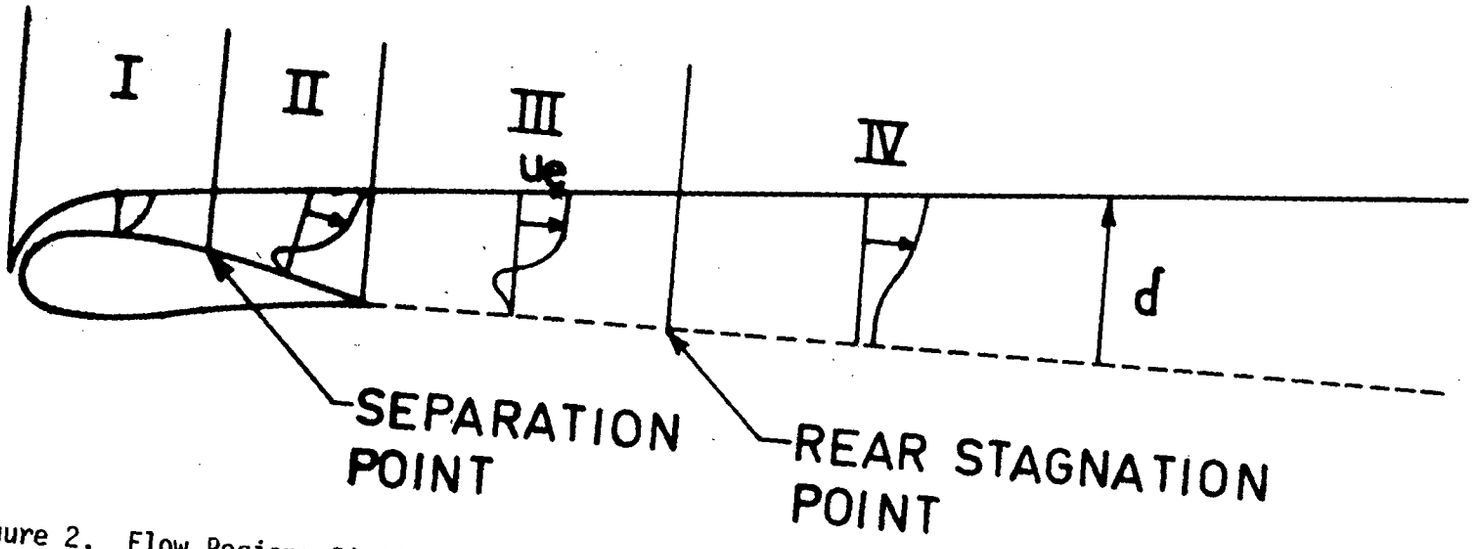

Figure 2. Flow Regions Distinguished by Velocity Profile Shape

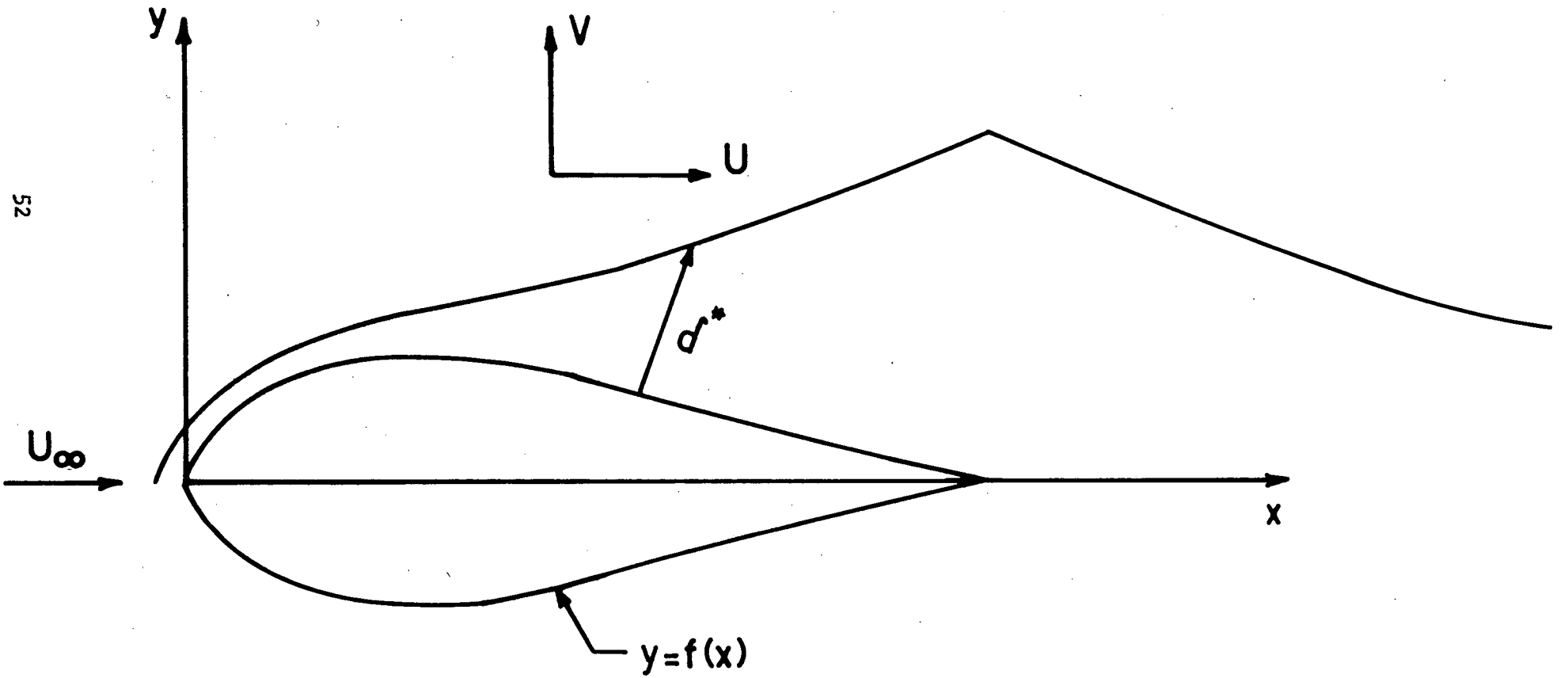

Figure 3. Coordinate System for Inviscid Region

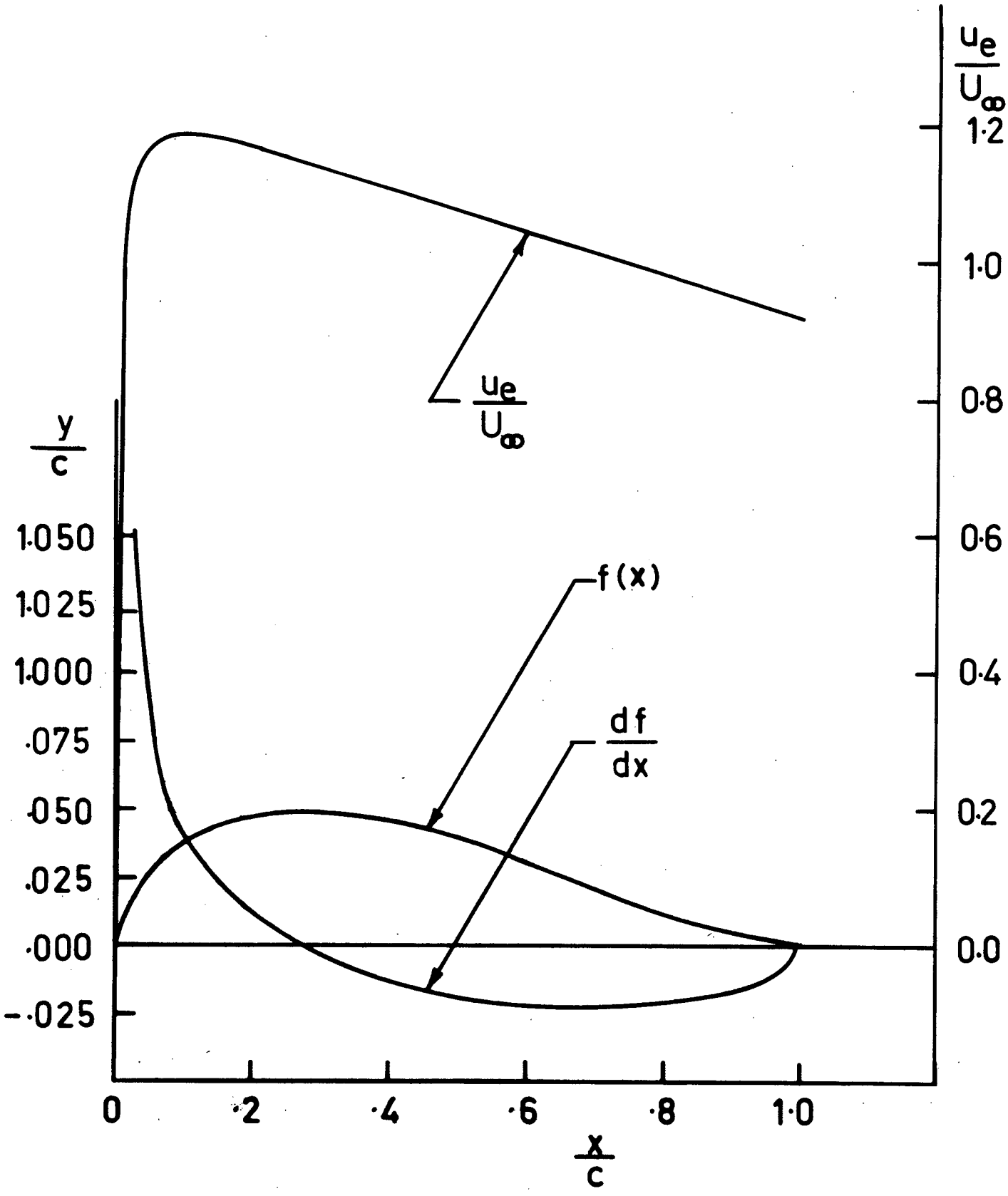

Figure 4. Joukowski Airfoil, Its Slope and Surface Speed

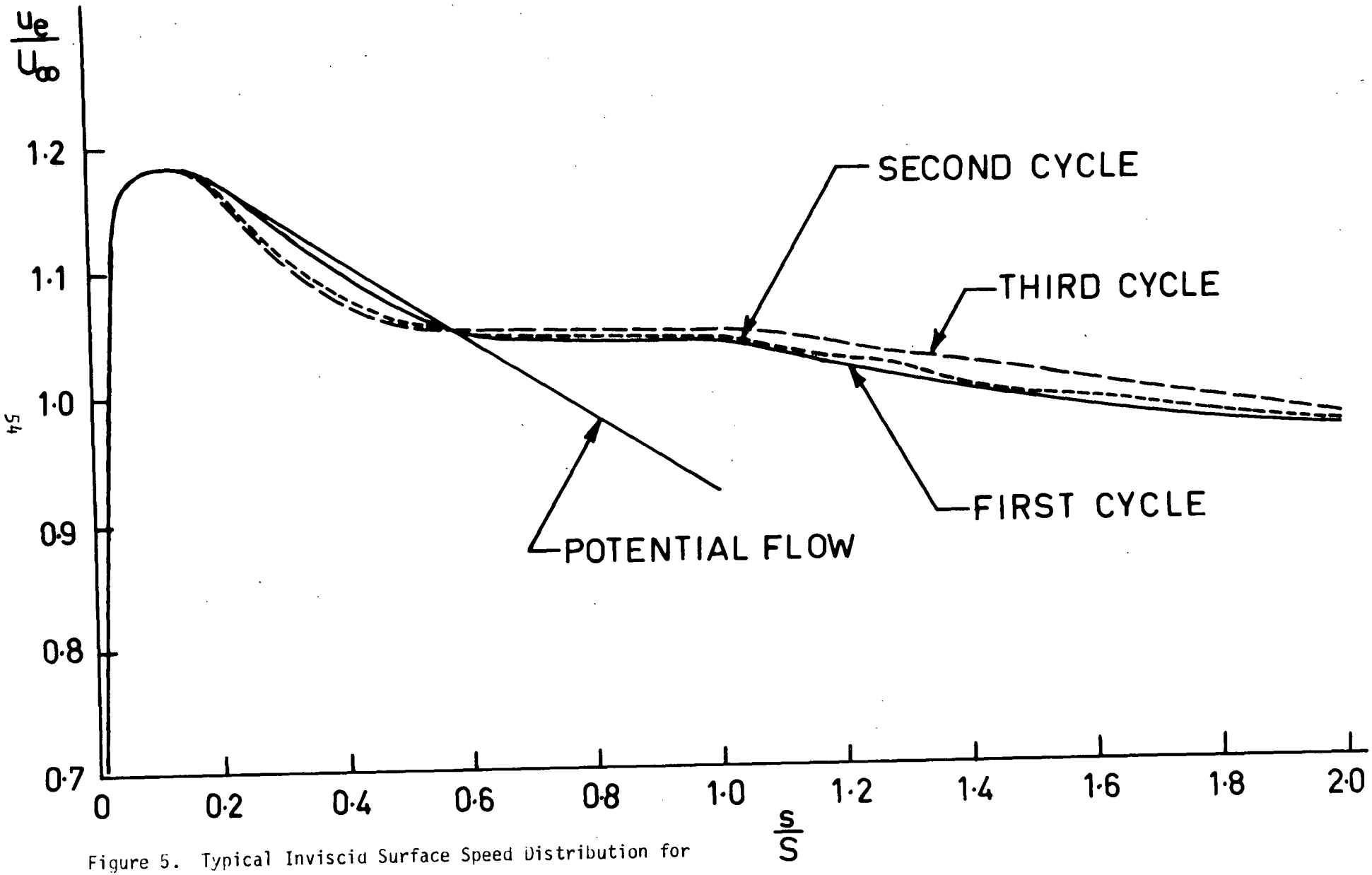

Figure 5. Typical Inviscid Surface Speed Distribution for Method of IIIA (On Airfoil)

Figure 6. Typical Inviscid Surface Speed Distribution for Method of IIIA (In Wake)

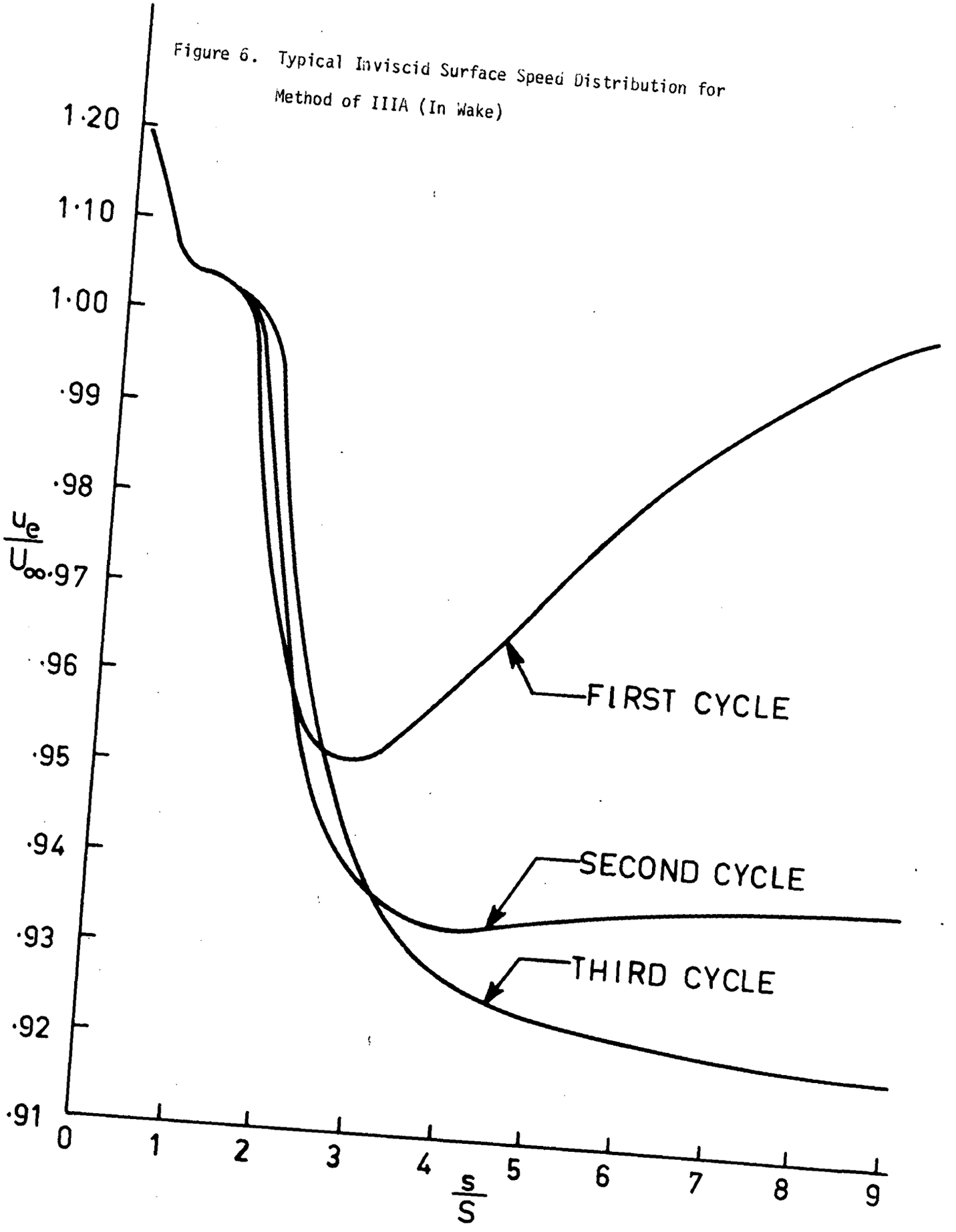

Figure 7. Typical tan θ Distribution for Method of IIIA

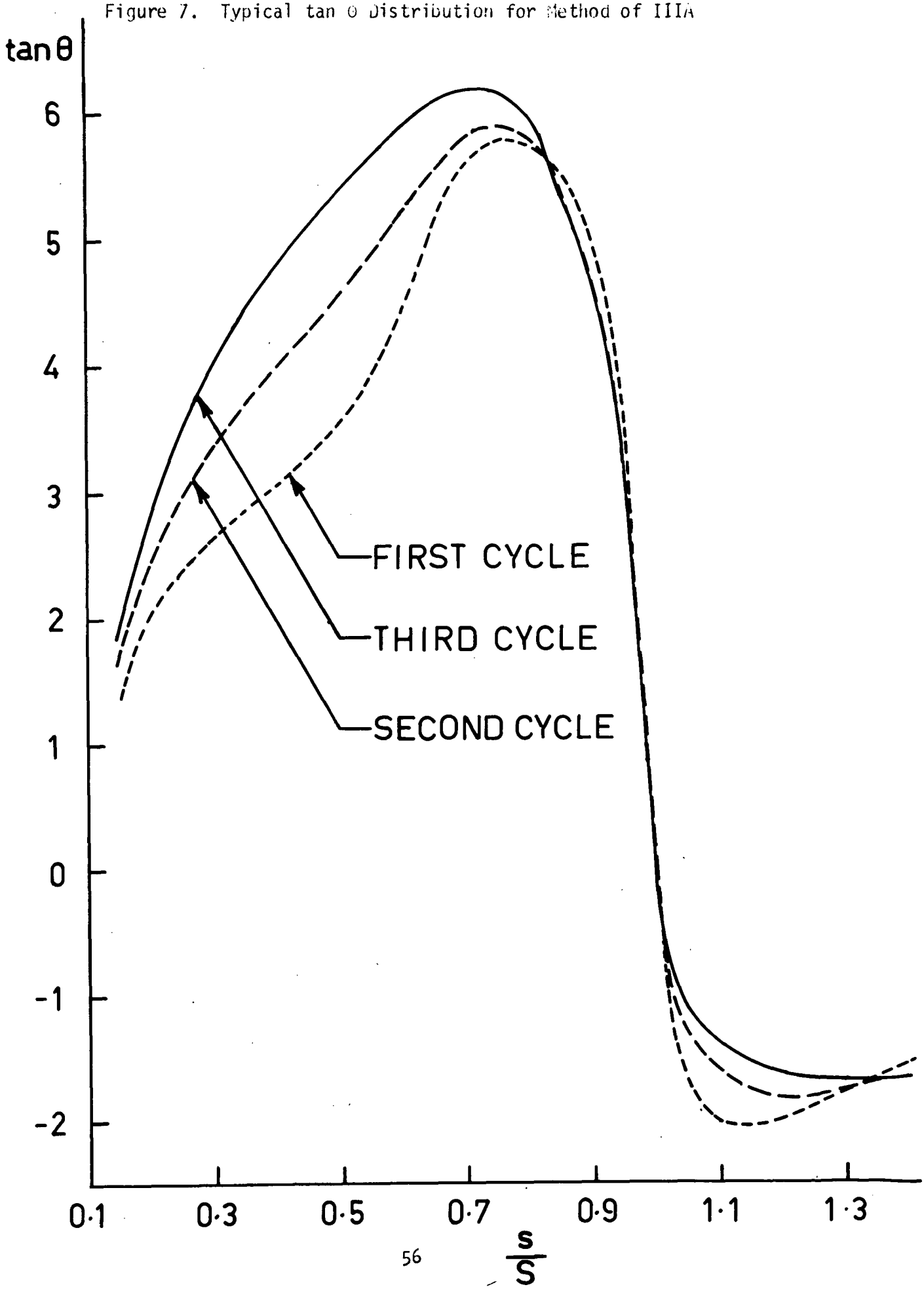

Figure 8. Typical Displacement Thickness Distribution for Method of IIIA (On Airfoil)

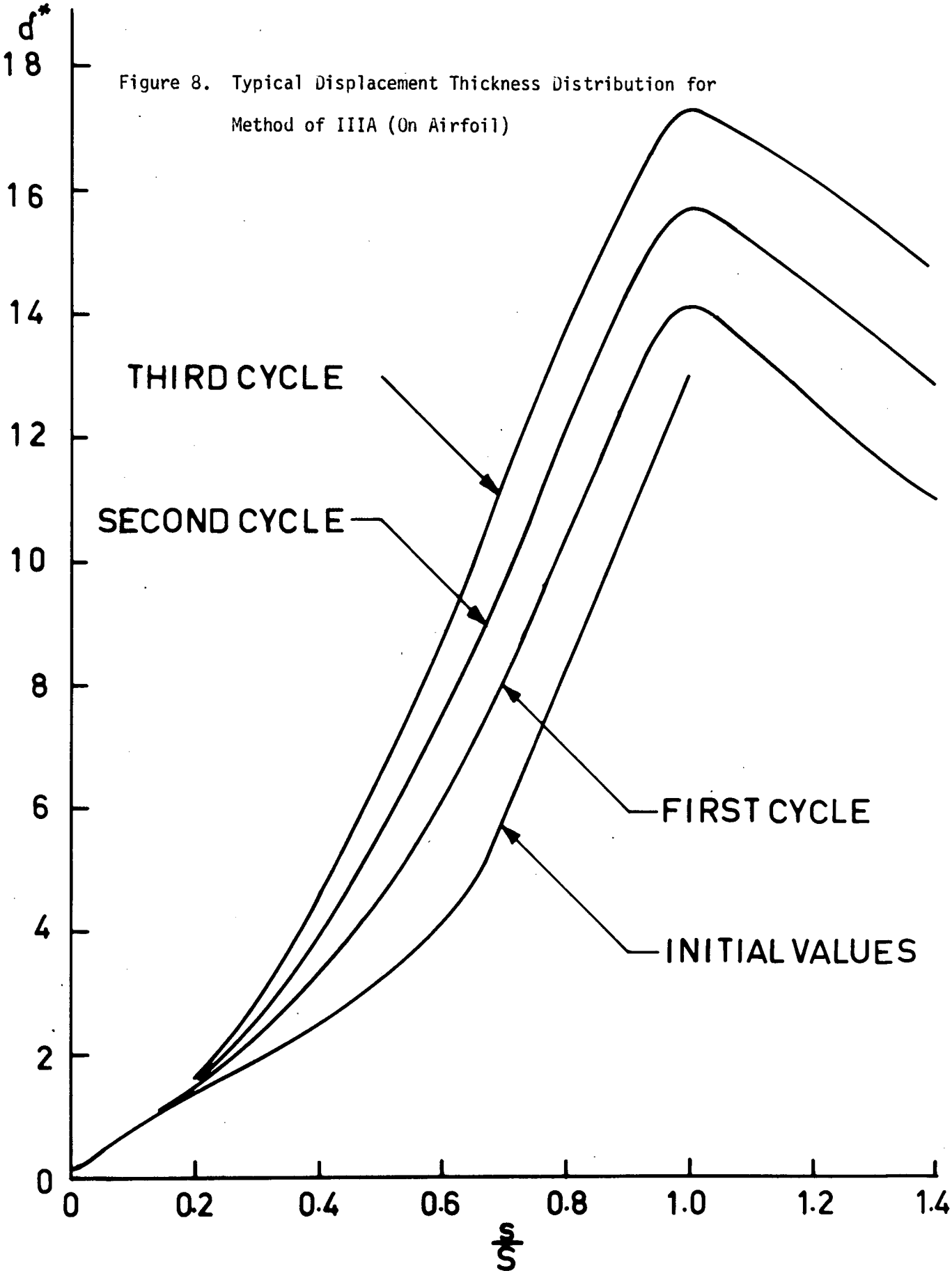

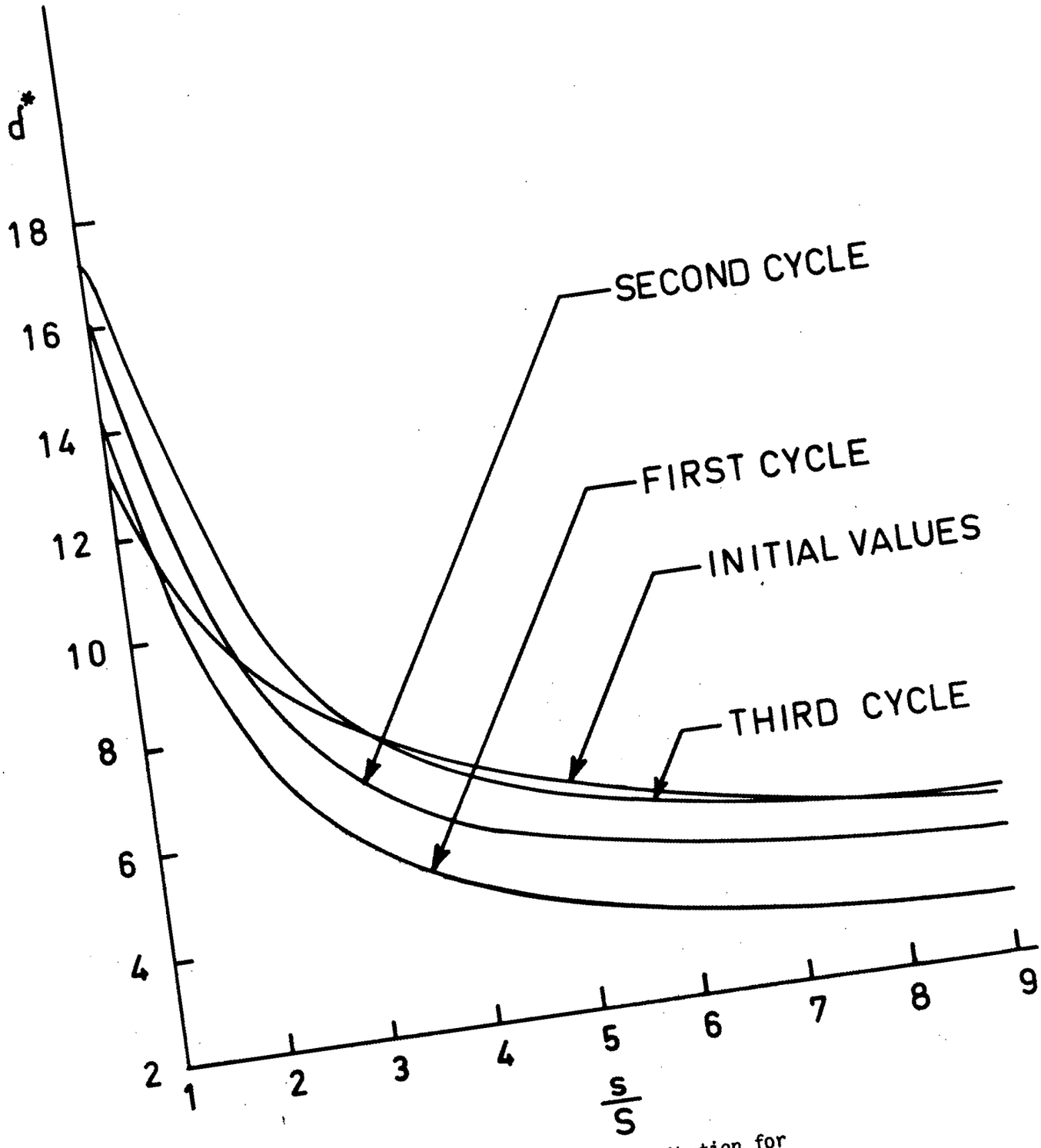

Figure 9. Typical Displacement Thickness Distribution for Method of IIIA (In Wake)

Figure 10. Solution of Weak Interaction Equations for Profile Parameter and Displacement Thickness

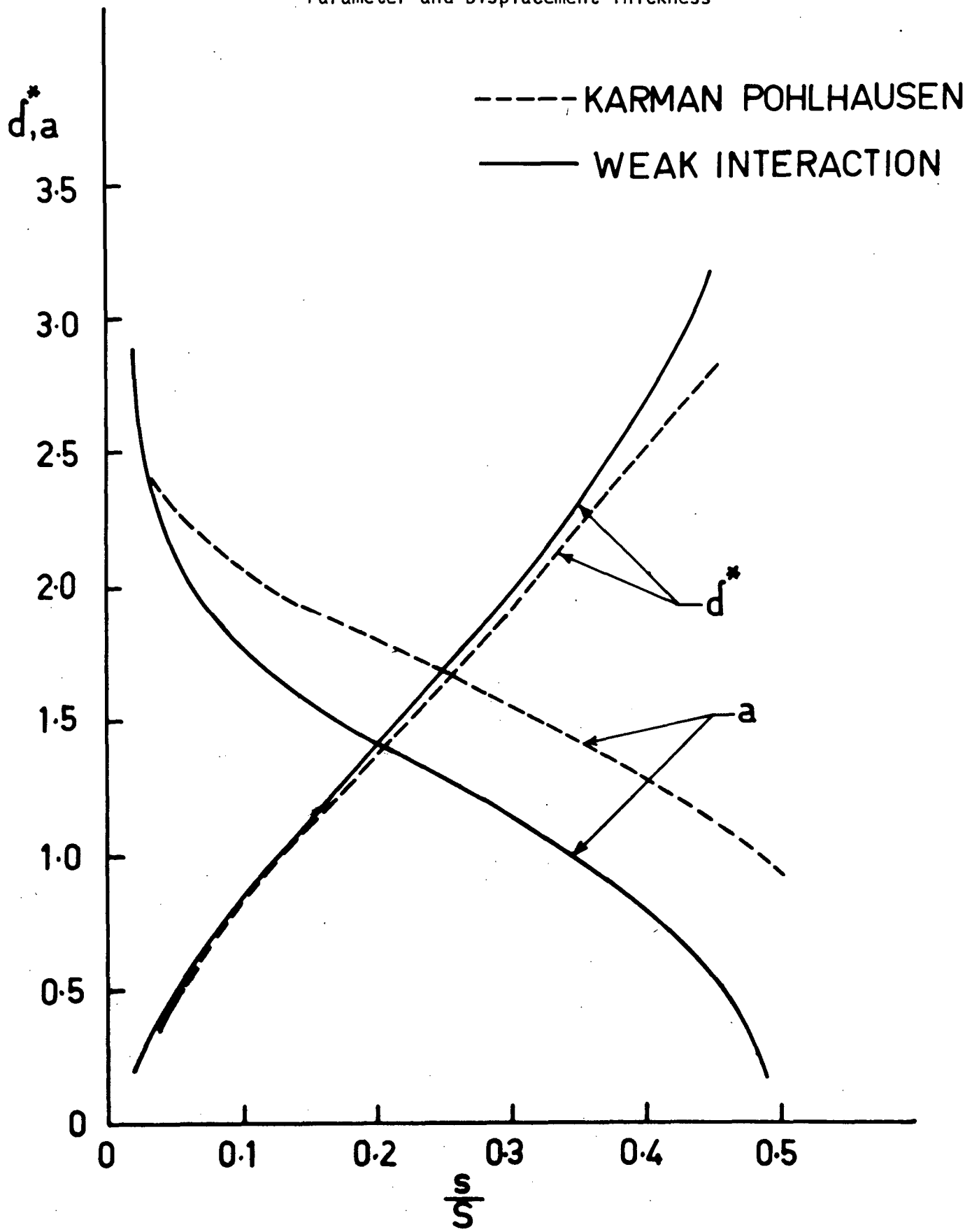

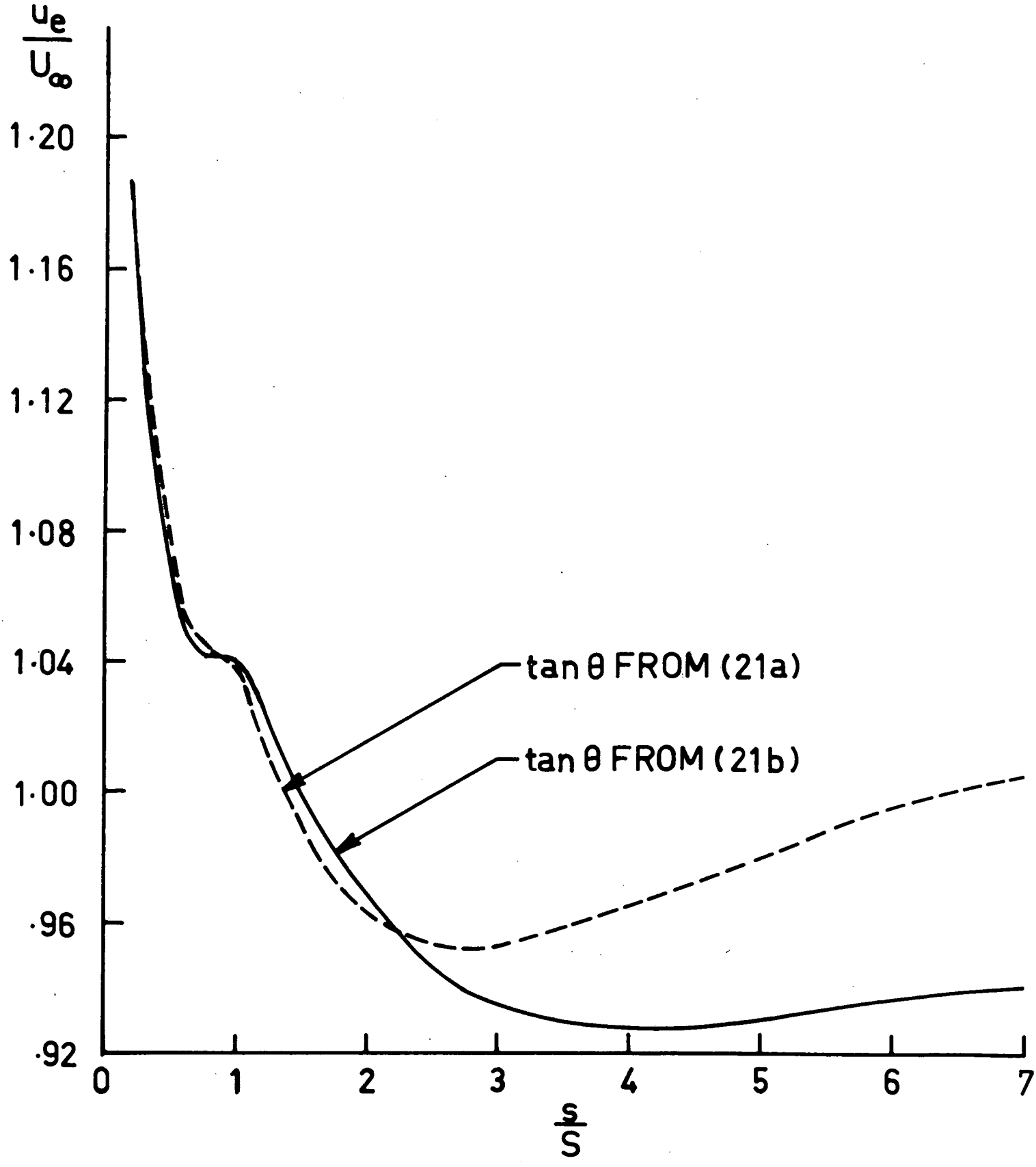

Figure 11. Inviscid Surface Speed Distributions Resulting from Initial tan θ Distributions of Equation (21)

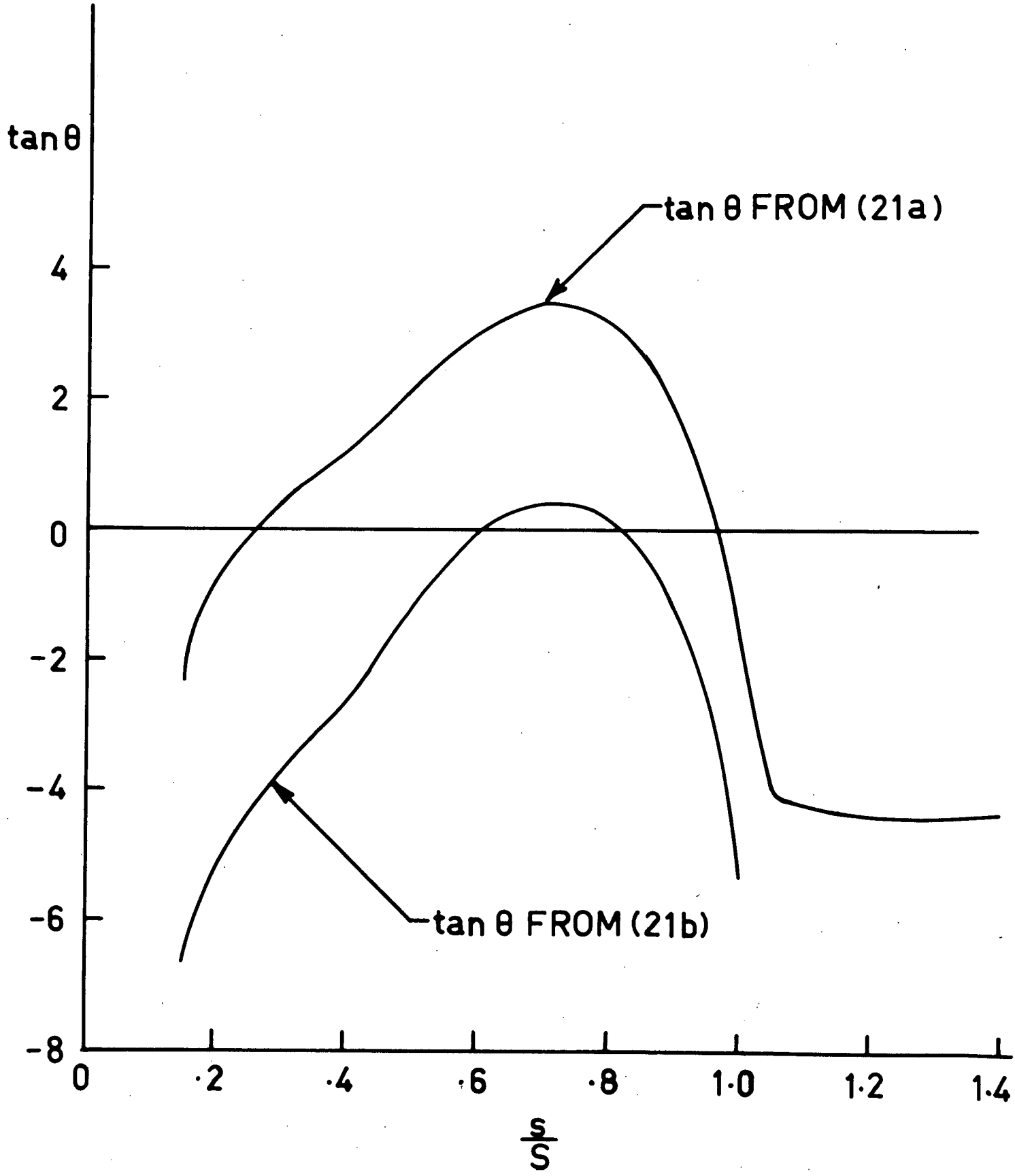

Figure 12. Updated tan Θ Distributions Resulting from Initial tan Θ Distributions of Equation (21)

Figure 13. Component Parts of tan θ Integral Shown in Figure 12

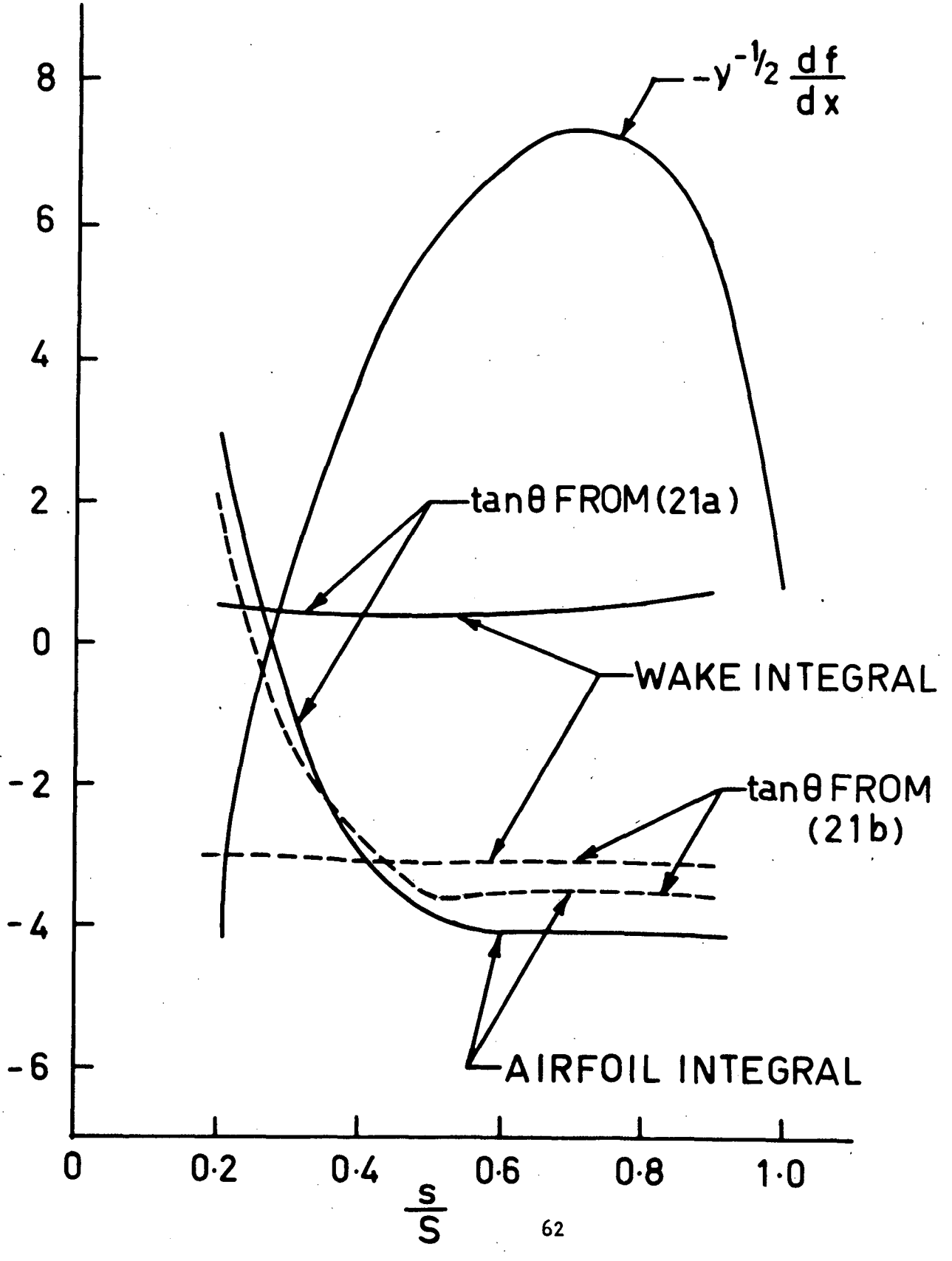

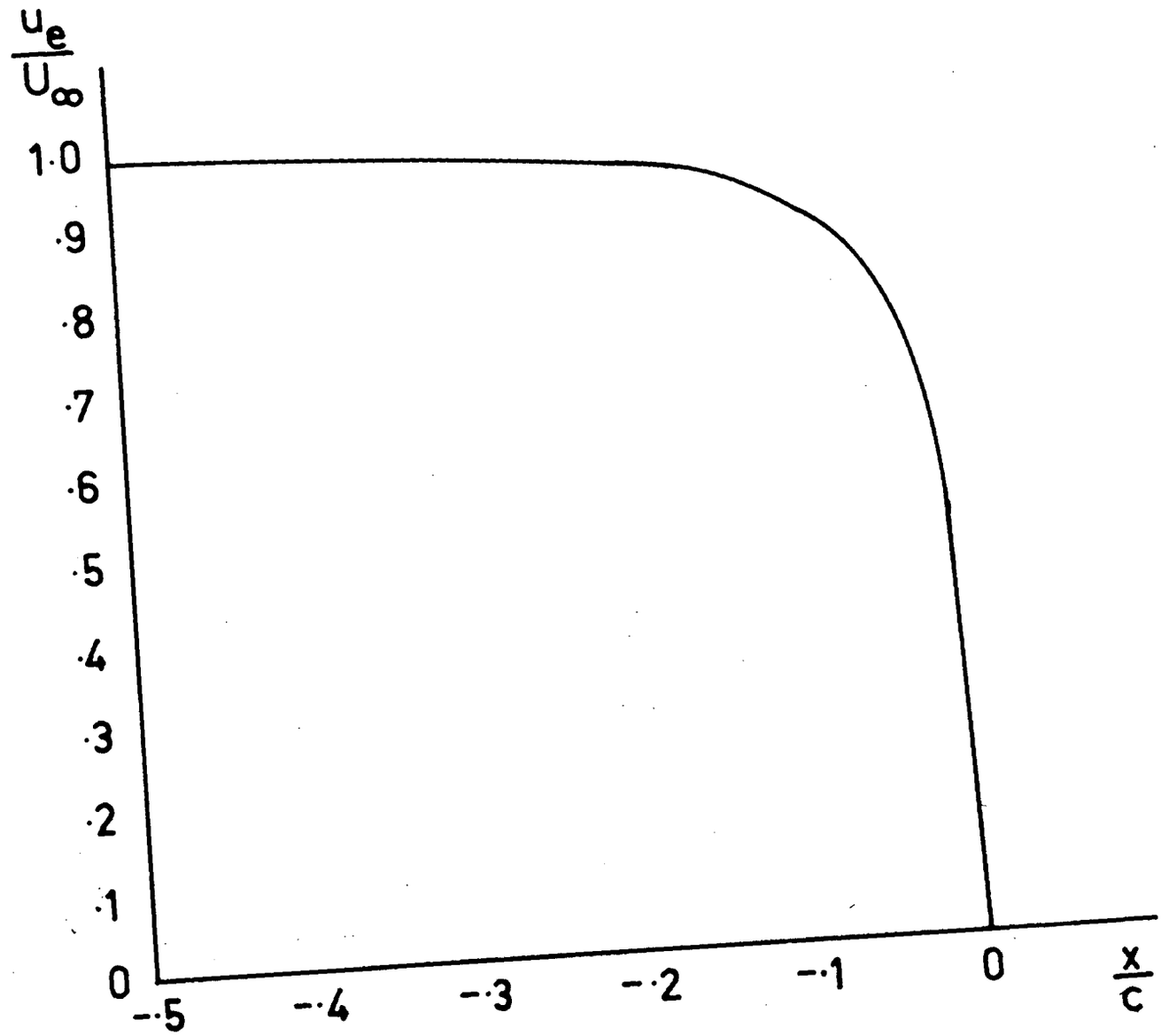

Figure 14. Potential Flow Surface Speed Distribution Upstream of Leading Edge

Figure 15. Updated tan θ Distribution Resulting from Initial tan θ Distribution of Equation (21b) Including Upstream Correction

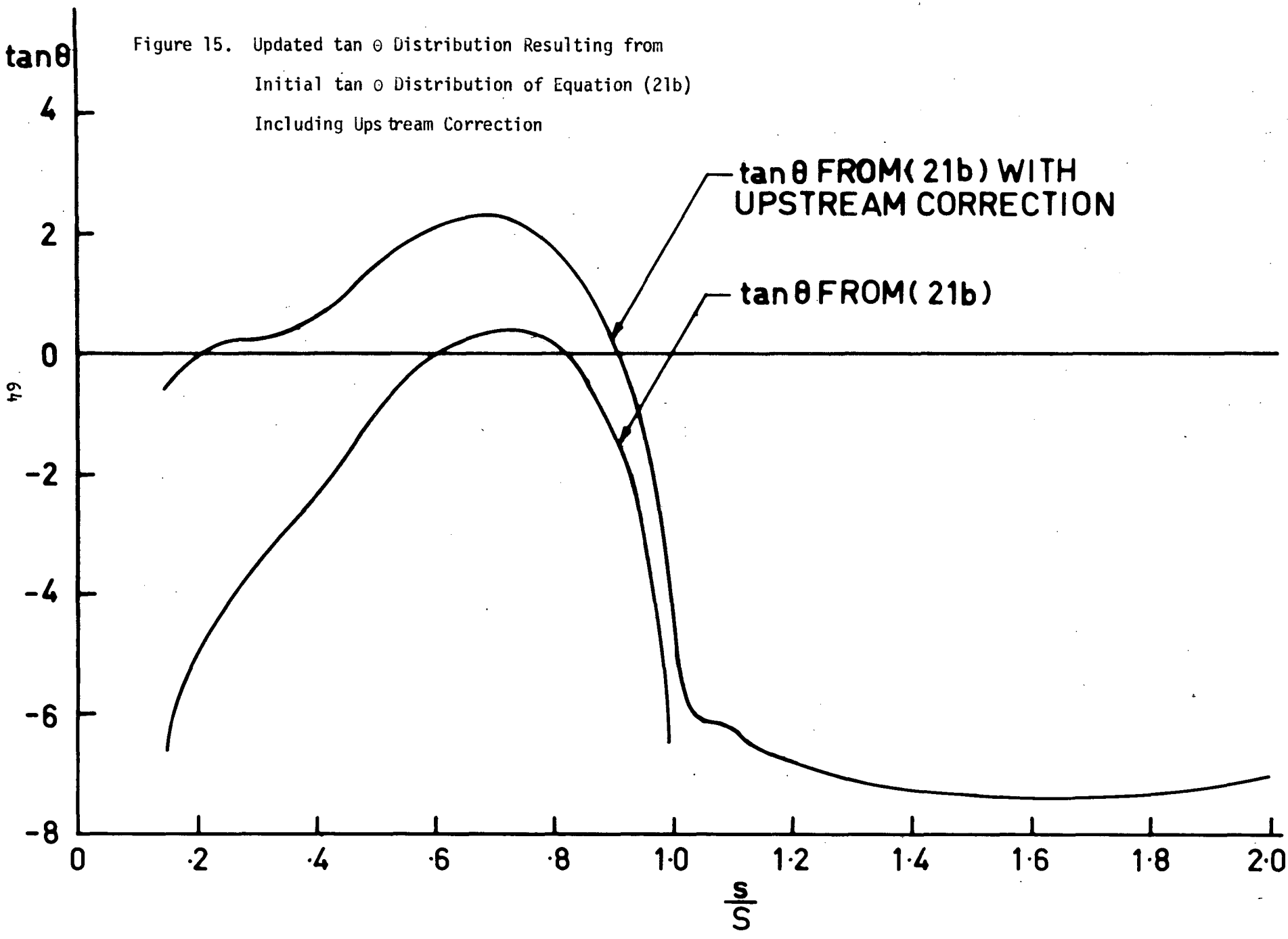

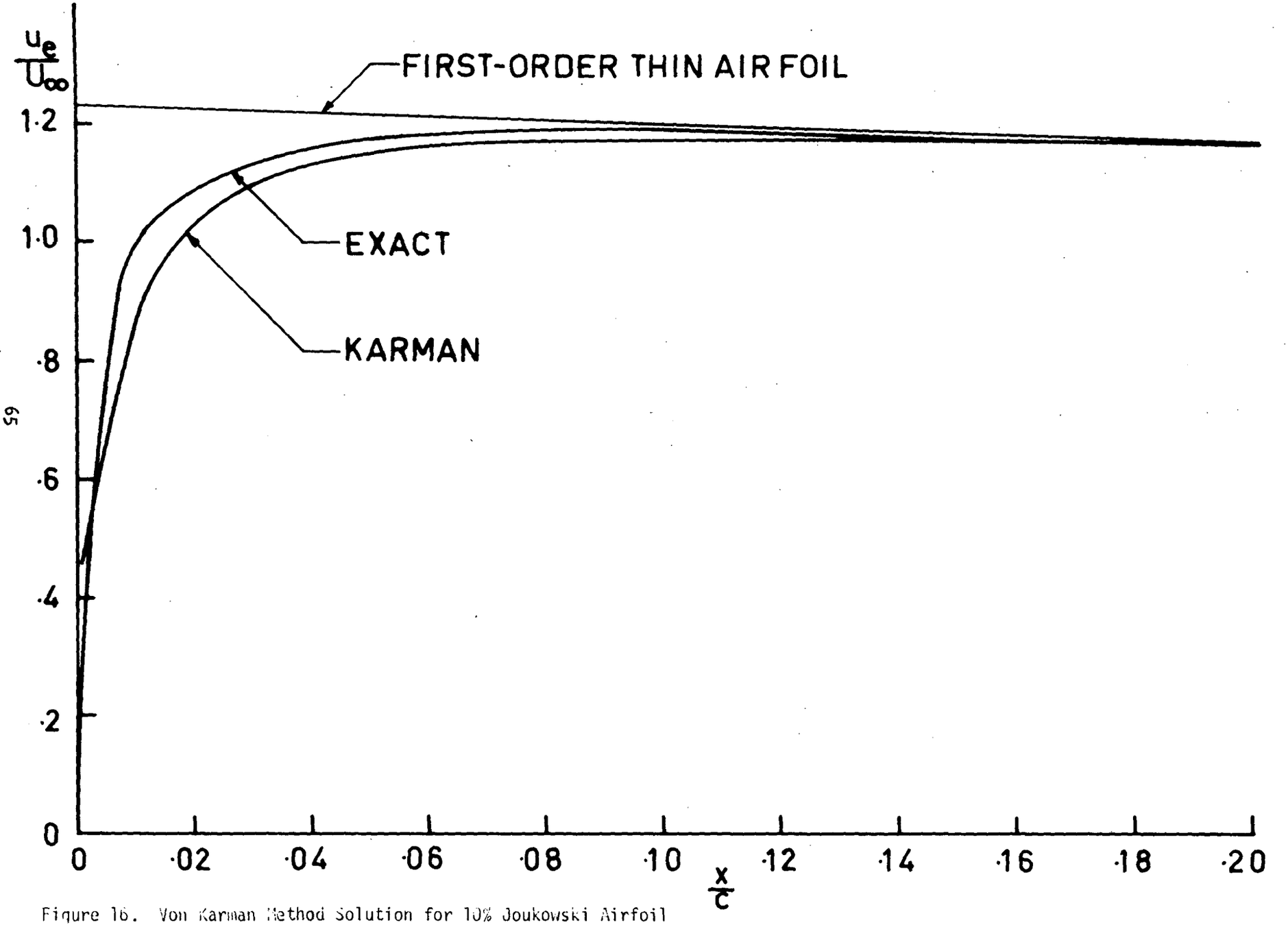

Figure 16. Von Karman Method Solution for 10% Joukowski Airfoil

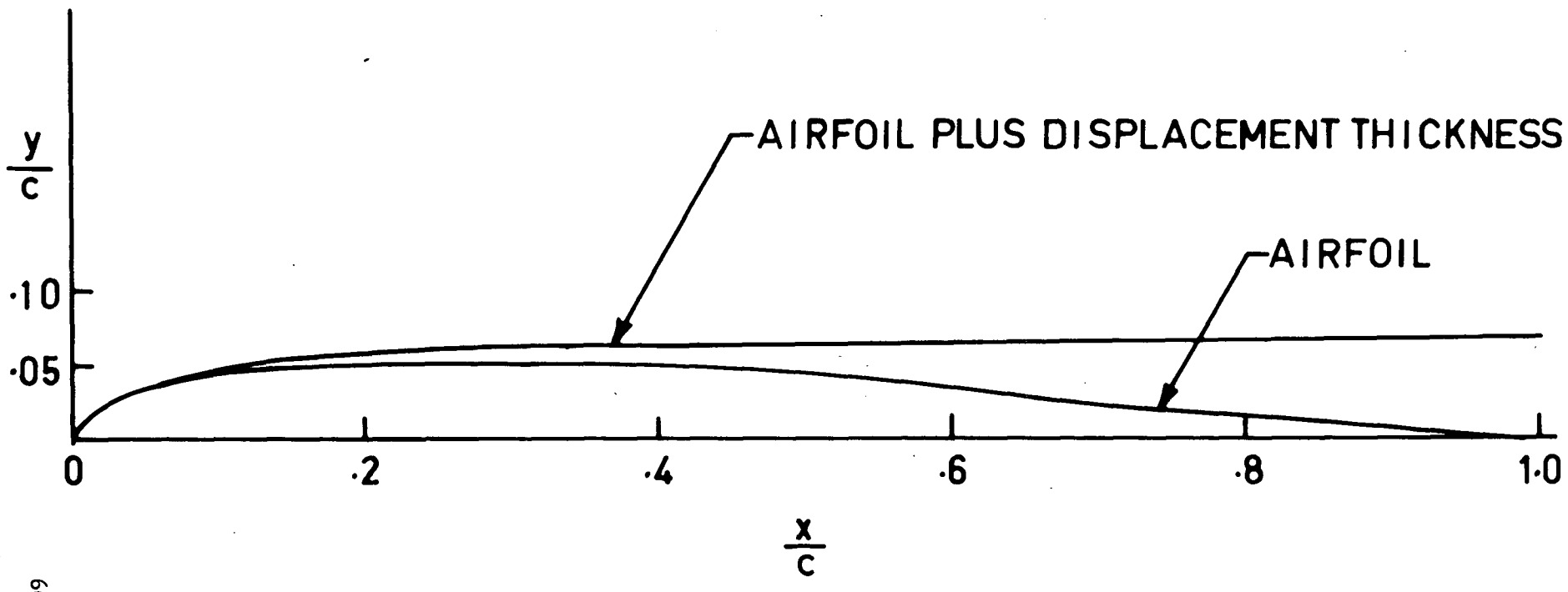

Figure 17. Typical Airfoil Plus Displacement Thickness for Method of IIID

Figure 18. Typical Displacement Thickness Distribution for Method of IIID

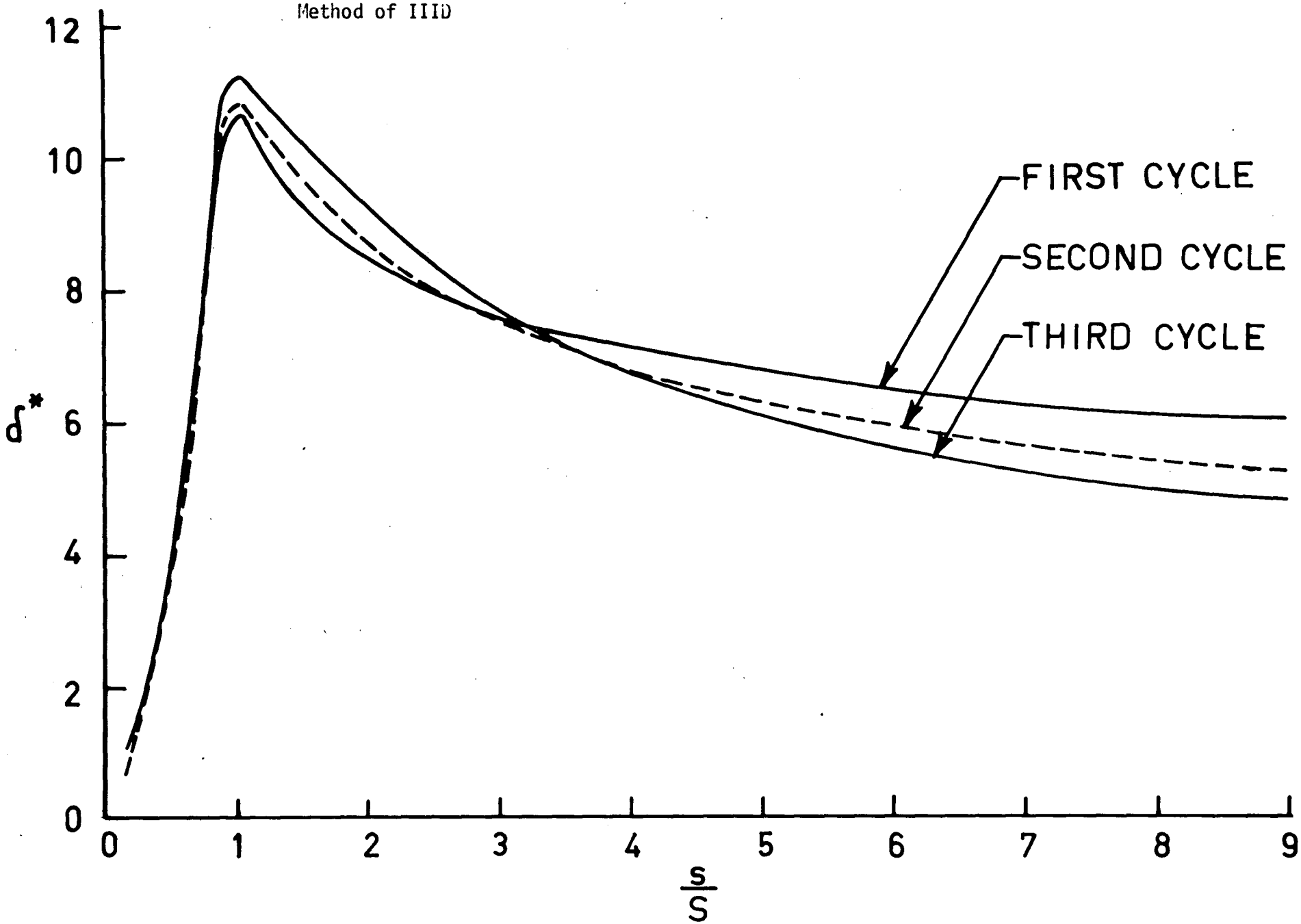

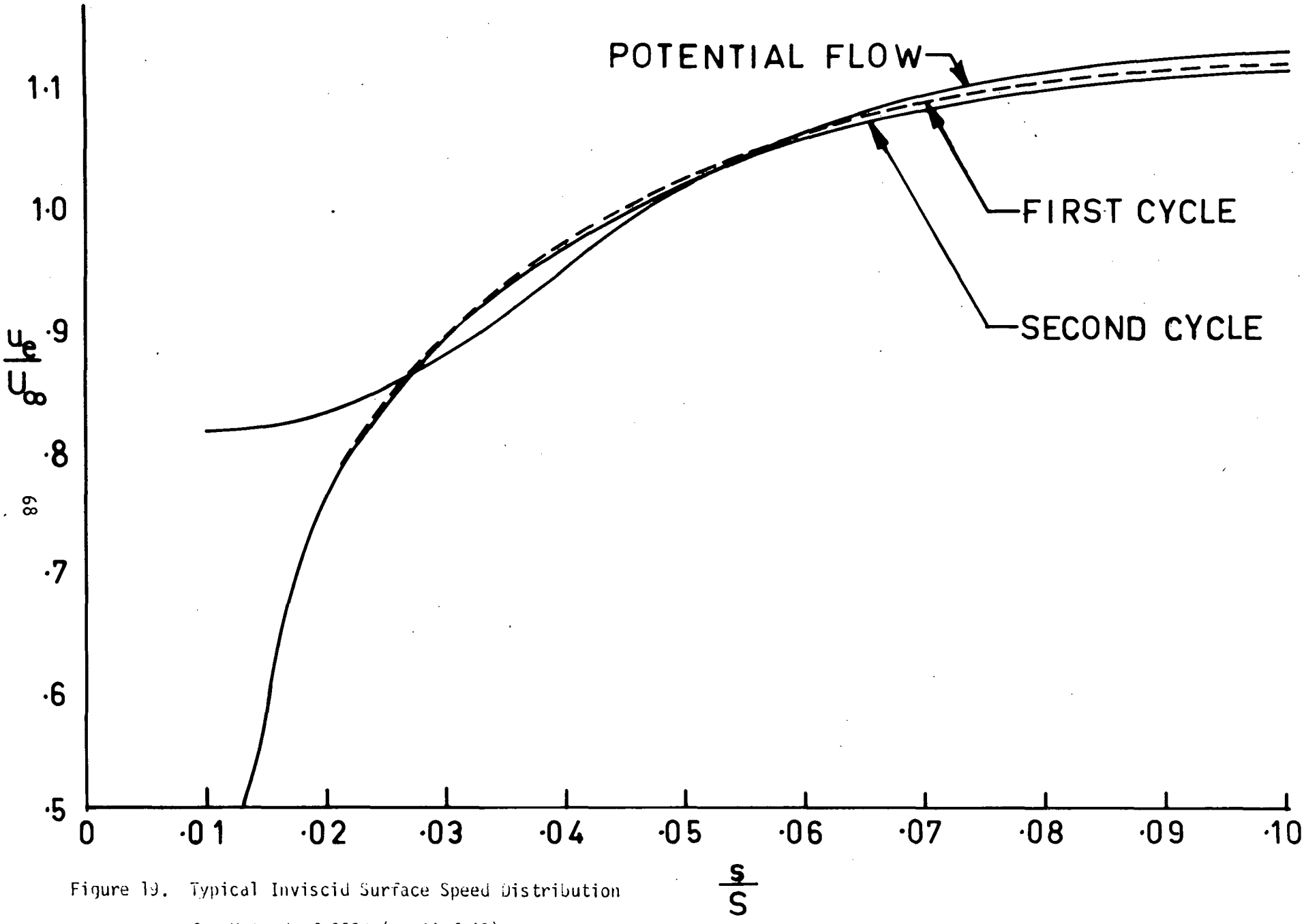

Figure 19. Typical Inviscid Surface Speed Distribution for Method of IIID (On Airfoil)

Figure 20. Typical Inviscid Surface Speed Distribution for Method of IIID (In Wake)

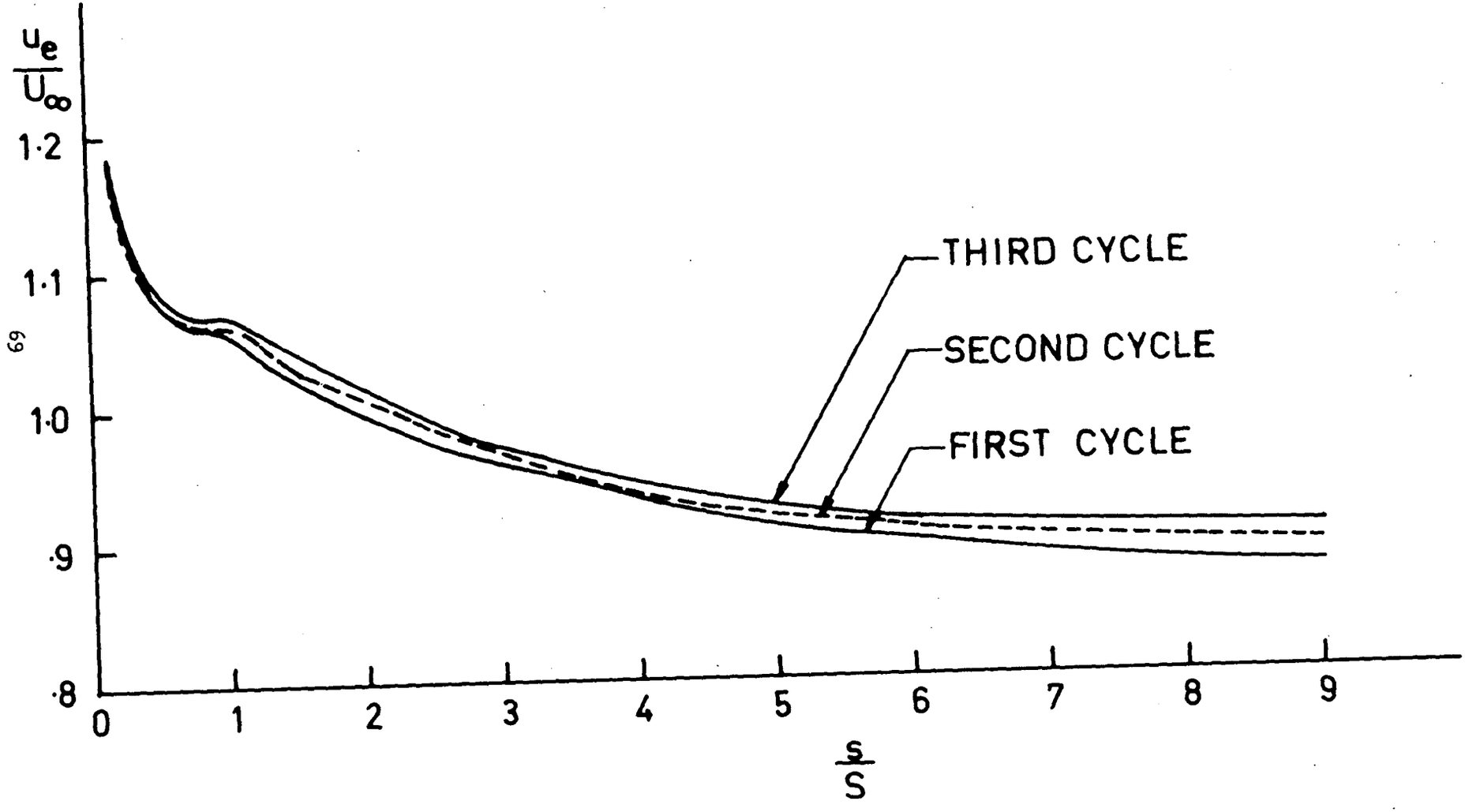

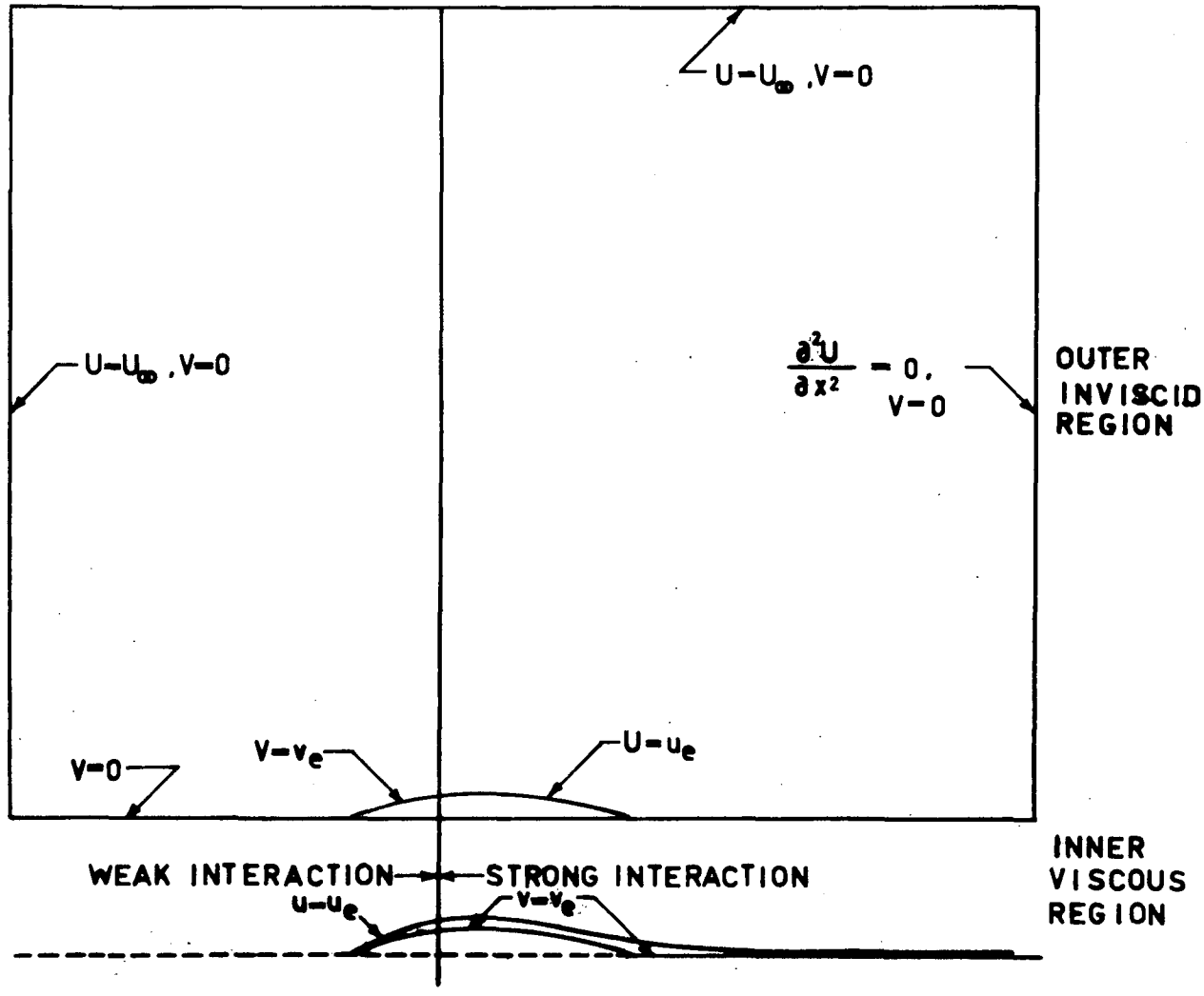

Figure 21. Computational Regions with Boundary Conditions for Method of Klineberg and Steger

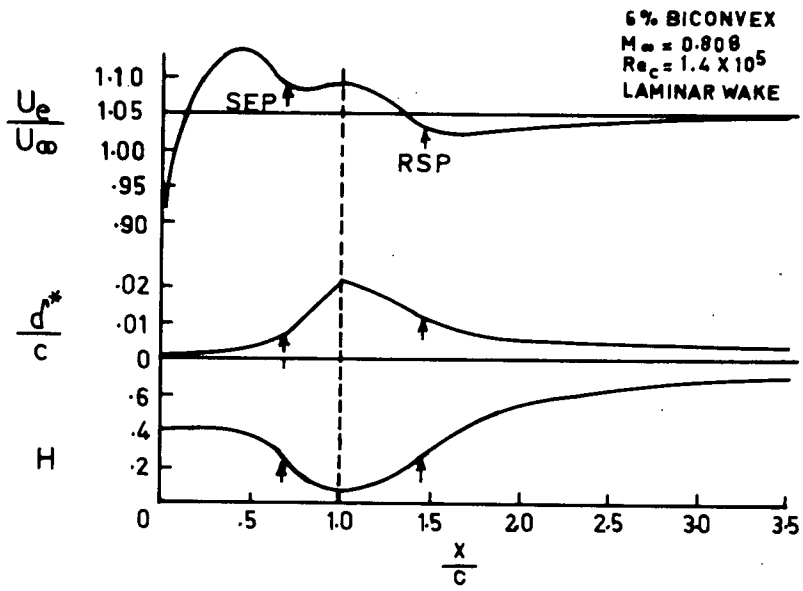

Figure 22. Typical Distributions for Method of Klineberg and Steger

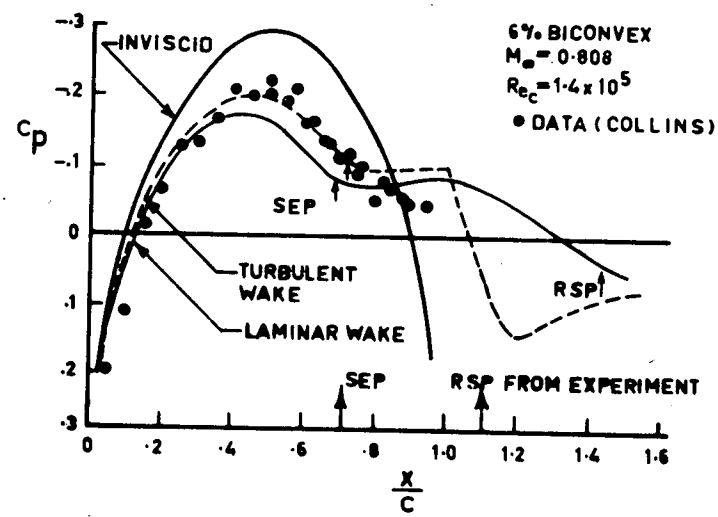

Figure 23. Comparison of Pressure Coefficient with Experimental Values of Collins for Method of Klineberg and Steger

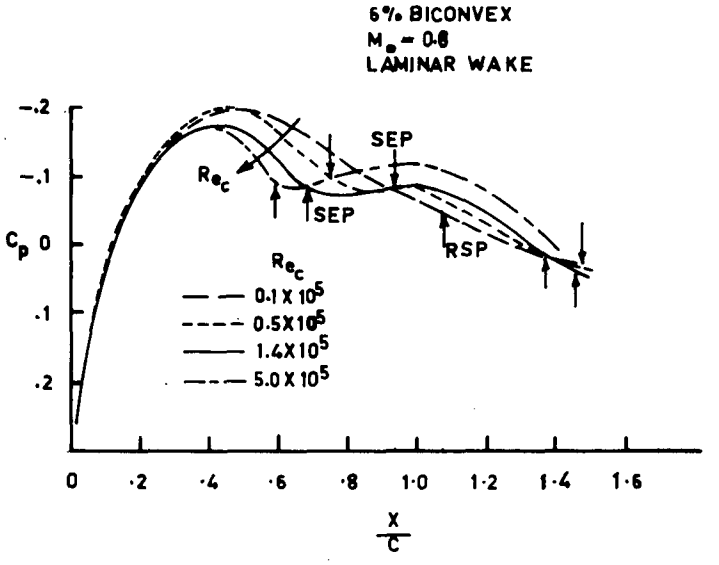

Figure 24. Effect of Reynolds Number on Pressure Coefficient for Method of Klineberg and Steger

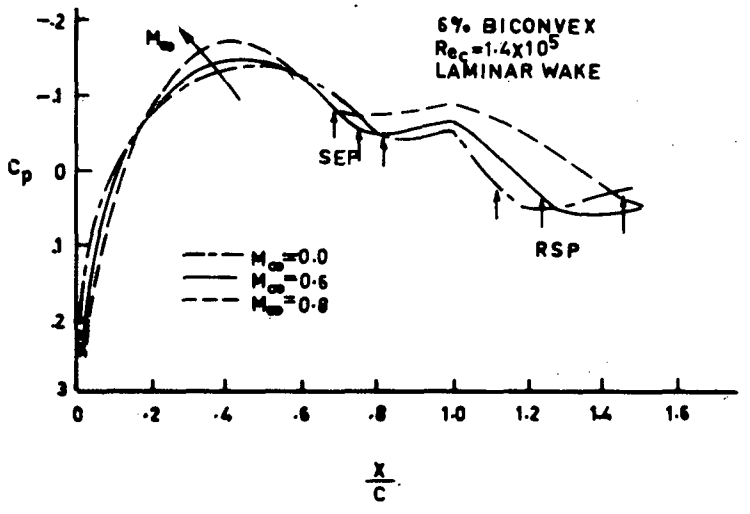

Figure 25. Effect of Mach Number on Pressure Coefficient for Method of Klineberg and Steger